

Generic no-scale inflation inspired from string theory compactifications

Lina Wu^{1,*} and Tianjun Li^{1,2,3,†}

¹*School of Sciences, Xi'an Technological University, Xi'an 710021, China*

²*CAS Key Laboratory of Theoretical Physics, Institute of Theoretical Physics, Chinese Academy of Sciences, Beijing 100190, China*

³*School of Physical Sciences, University of Chinese Academy of Sciences, No. 19A Yuquan Road, Beijing 100049, China*

Abstract

We propose the generic no-scale inflation inspired from string theory compactifications. We consider the Kähler potentials with an inflaton field φ , as well as one, two, and three Kähler moduli. Also, we consider the renormalizable superpotential of φ in general. We study the spectral index and tensor-to-scalar ratio in details, and find the viable parameter spaces which are consistent with the Planck and BICEP/Keck experimental data on the cosmic microwave background (CMB). The spectral index is $n_s \simeq 1 - 2/N \sim 0.965$ for all models, and the tensor-to-scalar ratio r is $r \simeq 12/N^2$, $83/N^4$ and $4/N^2$ for the one, two and three moduli models, respectively. The particular r for two moduli model comes from the contributions of the non-negligible higher order term in potential. In the three moduli model, the scalar potential is similar to the global supersymmetry, but the Kähler potential is different. The E-model with $\alpha = 1$ and T-model with $\alpha = 1/3$ can be realized in the one modulus model and the three moduli model, respectively. Interestingly, the models with quadratic and quartic potentials still satisfy the current tight bound on r after embedding into no-scale supergravity.

* wulina@xatu.edu.cn

† tli@itp.ac.cn

I. INTRODUCTION

It is well known that inflation solves several problems in the standard cosmology theory such as the horizon problem, flatness problem, and large structure of the Universe, etc [1–5]. The almost scale-invariant density perturbation spectrum predicted by inflation is qualitatively consistent with the cosmological observations, in particular, the cosmic microwave background radiation (CMB). With the advent of the era of precise cosmology, more and more observations have given or will give strong constraints on the inflationary models. From the Planck 2018 results on the CMB measurements [6], the scalar spectral index n_s , tensor-to-scalar ratio r , and scalar amplitude A_s for the power spectrum of the curvature perturbations are constrained to be $n_s = 0.9649 \pm 0.0042$, $r_{0.002} \leq 0.056$, and $A_s = 2.10 \times 10^{-9}$, respectively. Combining with BICEP/Keck data, the tensor-to-scalar ratio is further limited to $r_{0.05} \leq 0.036$ at 95% confidence level (C.L.) [7]. Such a tight bound on r is a big challenge to a lot of previously popular inflationary models. Interestingly, the inflationary models inspired from the string low-energy effective actions can have small tensor-to-scalar ratios $r < 0.01$ [8–12].

Supersymmetry provides a natural solution to the gauge hierarchy problem in the particle physics Standard Model (SM), and is the promising new physics beyond the SM. Especially, the scalar masses can be stabilized, and the superpotential is nonrenormalized. Thus, to stabilize the inflaton potential, we need to consider supersymmetry. Moreover, gravity plays an important role in the early Universe during inflation, so it seems to us that supergravity theory inspired from string theory is a natural framework for inflationary model building. However, supersymmetry breaking scalar masses are at the order of the gravitino mass in general, and then at the order of the Hubble parameter due to the large vacuum energy density during inflation. Thus, the slow-roll parameter η is at the order one $\mathcal{O}(1)$ during inflation, which conflicts with the slow-roll conditions. This gives rise to the so-called η problem [13–15]. As we know, there are a few elegant solutions: no-scale supergravity [16–24], shift symmetry in the Kähler potential [25–37], and helical phase inflation [38–41], etc.

No-scale supergravity has vanishing cosmological constant naturally, and then evades the Anti-de Sitter (AdS) vacua in the generic supergravity theory [16–18]. Interestingly, no-scale supergravity can be realized by the Calabi-Yau compactification with standard embedding of the weakly coupled heterotic $E_8 \times E_8$ theory [19], as well as by the similar compactification

of M-theory on S^1/Z_2 [20]. The Kähler potential of no-scale supergravity inspired by the above string theory compactifications [19, 20] is

$$K = -3\log(T + \bar{T} - 2|\varphi_i|^2) , \quad (1)$$

where T is the Kähler moduli, and φ_i denote the matter, Higgs and inflaton fields. In this paper, for simplicity, we shall neglect dilaton field and complex structure moduli, and only consider inflaton field φ in the following. Because Kähler potential is a logarithmic real function, the η problem is solved, and the inflaton potential can have flat directions as well. In particular, considering the no-scale supergravity and a Wess-Zumino superpotential, one can obtain the $R + R^2$ Starobinsky model elegantly [21, 22]. In addition to φ , T can be inflaton field as well [22, 23]. Of course, the predicted n_s and r are compatible with the CMB observations. For the relevant studies on string inflations, please see Refs. [42–50].

On the other hand, a generalized model named α -attractor inflation is build by introducing a parameter α related to the curvature of the inflaton Kähler manifold [51]. The inflationary attractors [11, 12, 52–58] such as T-models and E-models predict the tensor-to-scalar ratio r by a factor α , which are consistent with the current observations and can be tested in the future. In particular, to generalize the above no-scale inflation, one can introduce an α factor in the Kähler moduli

$$K = -3\alpha\log(T + \bar{T} - 2|\varphi|^2) , \quad (2)$$

and then study the unified no-scale attractors [55].

Because the above simple no-scale inflation is very interesting, we have strong motivation to study the generic no-scale inflation inspired by the string theory compactifications. The first question is what are the generic no-scale supergravity theories inspired by the string theory compactifications. Previously, one of us (T. L.) has already studied various orbifold compactifications of M-theory on T^6/Z_3 , T^6/Z_6 , T^6/Z_{12} , as well as the compactification by keeping singlets under $SU(2) \times U(1)$ symmetry, and then the compactification on S_1/Z_2 [59]. Thus, the generic no-scale inflation can be inspired by these compactifications. Inspired by the compactification by keeping singlets under $SU(2) \times U(1)$ symmetry and then the compactification on S^1/Z_2 [59], we can consider the Kähler potential with two Kähler moduli $T_{1,2}$ and one chiral field φ as follows

$$K = -2\log(T_1 + \bar{T}_1 - 2|\varphi|^2) - \log(T_2 + \bar{T}_2) . \quad (3)$$

Also, inspired by the orbifold compactifications of M-theory on T^6/Z_{12} and S^1/Z_2 [59], we can consider the Kähler potential with three Kähler moduli $T_{1,2,3}$ and one chiral field φ as follows

$$K = -\log(T_1 + \bar{T}_1 - 2|\varphi|^2) - \log(T_2 + \bar{T}_2) - \log(T_3 + \bar{T}_3) . \quad (4)$$

Previously, a few relevant studies have been done. A chaotic inflation in no-scale supergravity with string inspired moduli stabilization, which has two moduli, is obtained from Type IIB string compactification with an anomalous $U(1)_X$ gauged symmetry [60]. The tensor-to-scalar ratio is consistent with BICEP/Keck experimental data. In a recent paper [61] with Gong, we have studied the primordial black holes and secondary gravitational waves for the generic no-scale inflation with Kähler potentials in Eq. (3). However, the systematical studies on the generic no-scale inflation have not been done yet.

In this paper, we shall perform the systematical studies on the generic no-scale inflation with Kähler potentials in Eqs. (1), (3), and (4). We consider φ as an inflaton field, and the renormalizable superpotential of φ in general. We study the spectral index and tensor-to-scalar ratio in detail, and find the viable parameter spaces which are consistent with the Planck and BICEP/Keck experimental data on the cosmic microwave background (CMB). The spectral index is $n_s \simeq 1 - 2/N \sim 0.965$ for all models, and the tensor-to-scalar ratio is $r \simeq 12/N^2$, $83/N^4$ and $4/N^2$ for the one, two and three moduli models, respectively. The predicted r for two moduli models is clearly different from that for other two models due to the non-negligible higher order term, which will be explained in detail in Sec. V. In the three moduli model, the scalar potential is similar to the global supersymmetry, but the Kähler potential is different. The E-model with $\alpha = 1$ and T-model with $\alpha = 1/3$ can be realized in the one modulus model and the three moduli model, respectively. Interestingly, the models with quadratic and quartic potentials still satisfy the current tight bound on r after embedding into no-scale supergravity.

Based on the string compactifications, the coefficients of the logarithmic term are integers in Kähler potential. Thus, it is interesting to build the generic no-scale α -attractor inflation. We propose the following Kähler potential

$$K = -3\alpha \log(T + \bar{T} - 2|\varphi|^2) - 3(1 - \alpha) \log(T' + \bar{T}') , \quad (5)$$

where $0 < \alpha \leq 1$. From the phenomenological point of view, the generic attractor will relate the above three kinds of models with each other, and the predicted $n_s - r$ curves are

consistent with CMB experimental results. We shall preform the detailed study, which will be given elsewhere in the future.

This paper is organized as follows. We briefly discuss the generic no-scale supergravity theories inspired by the string theory compactifications in Sec. II. We show the generic slow-roll inflation model and field transformation in Sec. III. Then we study the cosmological predictions n_s and r for the inflationary models with one, two and three moduli in Secs. IV, V, and VI. Finally in Sec. VII, we make conclusions with a brief discussion. In the following, we set the reduced Planck mass $M_{\text{Pl}}^2 = 8\pi G = 1$ for simplicity.

II. THE GENERIC NO-SCALE SUPERGRAVITY THEORIES INSPIRED BY THE STRING THEORY COMPACTIFICATIONS

The Lagrangian of the $\mathcal{N} = 1$ supergravity can be written in the form

$$\mathcal{L} = -\frac{1}{2}R + K_i^{\bar{j}} \partial_\mu \varphi^i \partial^\mu \bar{\varphi}_{\bar{j}} - V, \quad (6)$$

where the Kähler metric is $K_i^{\bar{j}} \equiv \partial^2 K / (\partial \varphi^i \partial \bar{\varphi}_{\bar{j}})$. The effective scalar potential is

$$V = e^G \left[\frac{\partial G}{\partial \varphi^i} (K^{-1})^i_{\bar{j}} \frac{\partial G}{\partial \bar{\varphi}_{\bar{j}}} - 3 \right], \quad (7)$$

where the Kähler function is $G \equiv K + \ln |W|^2$, and $(K^{-1})^i_{\bar{j}}$ is the inverse of the Kähler metric. Introducing Kähler covariant derivative

$$D_i W \equiv W_i + K_i W, \quad (8)$$

we obtain the scalar potential

$$V = e^K \left[D_i W (K^{-1})^i_{\bar{j}} D^{\bar{j}} \bar{W} - 3|W|^2 \right]. \quad (9)$$

To study the inflation in the generic no-scale supergravity theories inspired by the string theory compactifications, we parametrize the generic Kähler potential and superpotential as follows:

$$K = -N_1 \log(T_1 + \bar{T}_1 - 2|\varphi|^2) - \sum_{i=2,3} N_i \log(T_i + \bar{T}_i), \quad (10)$$

$$W = \sum_{i=0}^3 a_i (\sqrt{2}\varphi)^i, \quad (11)$$

where $N_1 + N_2 + N_3 = 3$, T_i are Kähler moduli, and φ is inflaton field. According to the number of Kähler moduli T_i , we shall classify the inflationary models as one moduli model, two moduli model, and three moduli model [61]. We also consider $W_T = 0$, and the η problem is avoided since no large mass term is generated [62, 63]. For simplicity, we assume inflation along the $\text{Re}(\varphi)$ direction as well. Moreover, the Kähler metric and covariant derivative are

$$K_i^{\bar{j}} = \begin{pmatrix} \frac{N_1}{X^2} & 0 & 0 & -\frac{2N_1\varphi}{X^2} \\ 0 & \frac{N_2}{Y_2^2} & 0 & 0 \\ 0 & 0 & \frac{N_3}{Y_3^2} & 0 \\ -\frac{2N_1\bar{\varphi}}{X^2} & 0 & 0 & \frac{2N_1Y_1}{X^2} \end{pmatrix} \quad (12)$$

$$D_i W = W \left(-\frac{N_1}{X} \quad -\frac{N_2}{Y_2} \quad -\frac{N_3}{Y_3} \quad \frac{2N_1\bar{\varphi}}{X} + \frac{W_\varphi}{W} \right) \quad (13)$$

where $X \equiv T_1 + \bar{T}_1 - 2|\varphi|^2$, $Y_i \equiv T_i + \bar{T}_i$. Thus, the general scalar potential can be written as

$$V = \frac{|W_\varphi|^2}{2N_1 X^{N_1-1} Y_2^{N_2} Y_3^{N_3}}. \quad (14)$$

In the following section, we will study inflationary models with typical Kähler potential in the general no-scale supergravity model. Then we will compare the predictions of these models with CMB observations in order to find the observational constraints on the parameter space of the models.

III. INFLATIONARY MODELS

We assume that all the real components of the complex fields which do not drive inflation have been stabilized, whereas the inflaton field remains dynamical. Following Refs. [21, 22, 64–66], the real and imaginary parts of modulus T_i can be stabilized by adding $(T_i + \bar{T}_i - 1)^4$ terms and $(T_i - \bar{T}_i)^4$ terms into the log terms of the Kähler potential. In this paper, we fix the moduli T_i with vacuum expectation values (VEVs) $2\langle \text{Re}(T_i) \rangle = c_i$ and $\langle \text{Im}(T_i) \rangle = 0$. Also, without loss of generality, we assume the inflation trajectory along the real part of the φ direction. The scalar potential in the Jordan frame is

$$V = V_0 \frac{|W_\varphi|^2}{(c_1 - 2|\varphi|^2)^{N_1-1}}, \quad (15)$$

where $V_0 = 1/(2N_1 c_2^{N_2} c_3^{N_3})$. The inflationary model with $N_1 = 1$ is similar to that with the global supersymmetry.

The kinetic term in terms of the field φ in Eq. (6) is noncanonical, so we need to define a new canonical field χ , which satisfies

$$\frac{1}{2}\partial_\mu\chi\partial^\mu\chi = K_{\varphi\bar{\varphi}}\partial_\mu\varphi\partial^\mu\bar{\varphi} \quad (16)$$

with

$$K_{\varphi\bar{\varphi}} = \frac{2N_1(T_1 + \bar{T}_1)}{(T_1 + \bar{T}_1 - 2|\varphi|^2)^2}. \quad (17)$$

By integrating the above equation, we get the field transformation

$$\varphi = \sqrt{\frac{c_1}{2}} \tanh\left(\frac{\chi}{\sqrt{2N_1}}\right). \quad (18)$$

Then the scalar potential in the Einstein frame is

$$V = V_1 \text{sech}^{2m}(b\chi) \left(a_1 + 2a_2\sqrt{c_1} \tanh(b\chi) + 3a_3c_1 \tanh^2(b\chi)\right)^2 \quad (19)$$

where $V_1 = N_1^{-1}c_1^m c_2^{-N_2} c_3^{-N_3}$ and $b = 1/\sqrt{2N_1}$, $m = 1 - N_1$. Furthermore, the T-model and E-model [51] will be realized by setting $N_1 = 1$ with $a_1 = a_3 = 0$ and $N_1 = 3$ with $a_1 = 0$, respectively. Defining $\varphi = (\phi + i\xi)/\sqrt{2}$ and taking T-models for example, the squared masses of ξ are $m_\xi^2 = 8a_2^2/(c_2c_3)$ for the φ^2 model and $m_\xi^2 = 36a_3^2\phi^2/(c_2c_3)$ for the φ^4 model.

In the following calculations, the new canonical field χ is regarded as inflaton. The slow-roll parameters are

$$\varepsilon(\chi) = \frac{M_{\text{Pl}}^2}{2} \left(\frac{V_\chi}{V}\right)^2, \quad \eta(\chi) = M_{\text{Pl}}^2 \frac{V_{\chi\chi}}{V} \quad (20)$$

The CMB observations in terms of slow-roll parameters are $n_s = 1 - 2\varepsilon + 6\eta$ and $r = 16\varepsilon$. Under the slow-roll approximation, the power spectrum can be expressed by

$$A_s = \frac{1}{24\pi^2 M_{\text{Pl}}^2} \frac{V}{\varepsilon}, \quad (21)$$

and is fixed to 2.10×10^{-9} by choosing the proper parameter V_0 in our calculations.

IV. ONE MODULUS INFLATIONARY MODEL

The simple no-scale supergravity model with one modulus [16, 18] can be realized via the Calabi-Yau compactification with standard embedding of the weakly coupled heterotic $E_8 \times E_8$ theory [19] and M-theory on S^1/Z_2 [20]. Assuming Kähler potential of the form

$$K = -3 \ln(T + \bar{T} - 2|\varphi|^2) \quad (22)$$

and substituting $N_1 = 3$ and $N_2 = N_3 = 0$ into Eq. (14), the scalar potential in the Jordan frame and the Einstein frame become

$$\begin{aligned} V &= \frac{|W_\varphi|^2}{6(c_1 - 2|\varphi|^2)^2} \\ &= V_0 e^{-2\sqrt{\frac{2}{3}}\chi} \left(1 + A_1 e^{\sqrt{\frac{2}{3}}\chi} + B_1 e^{2\sqrt{\frac{2}{3}}\chi} \right)^2, \end{aligned} \quad (23)$$

where $V_0 = \frac{(a_1 - 2a_2\sqrt{c_1} + 3a_3c_1)^2}{48c_1^2}$, $A_1 = \frac{2(a_1 - 3a_3c_1)}{a_1 - 2a_2\sqrt{c_1} + 3a_3c_1}$, and $B_1 = \frac{a_1 + 2a_2\sqrt{c_1} + 3a_3c_1}{a_1 - 2a_2\sqrt{c_1} + 3a_3c_1}$.

A. Zero parameter models

First, we consider the inflationary case only with one term in the numerator of the potential (23), which can be rewritten as

$$\begin{aligned} a_1 = a_2 = 0; V &= 3a_3^2 \sinh^4 \left(\frac{\chi}{\sqrt{6}} \right), \\ a_1 = a_3 = 0; V &= \frac{a_2^2}{3c} \sinh^2 \left(\sqrt{\frac{2}{3}}\chi \right), \\ a_2 = a_3 = 0; V &= \frac{a_1^2}{3c^2} \cosh^4 \left(\frac{\chi}{\sqrt{6}} \right). \end{aligned} \quad (24)$$

The minimum of potential is at $\chi_m = 0$ and inflation will occur on the left or right branches. However, in these models, the second order slow-roll parameters are

$$\begin{aligned} a_1 = a_2 = 0; \eta(\chi) &= 2 \coth^2 \left(\frac{\chi}{\sqrt{6}} \right) + \frac{2}{3}, \\ a_1 = a_3 = 0; \eta(\chi) &= \frac{4}{3} \left(\coth^2 \left(\sqrt{\frac{2}{3}}\chi \right) + 1 \right), \\ a_2 = a_3 = 0; \eta(\chi) &= 2 \tanh^2 \left(\frac{\chi}{\sqrt{6}} \right) + \frac{2}{3}. \end{aligned} \quad (25)$$

Therefore, inflation is unbearable since slow-roll conditions $\varepsilon, |\eta| \ll 1$ are unsatisfied and $\eta \rightarrow 8/3$ in the limit $\chi \rightarrow \infty$.

B. $a_1 = 0$ case: $A_1 + B_1 = -1$

For $a_1 = 0$, the two parameters A_1 and B_1 relate with each other as $A_1 + B_1 = -1$, and defining a new parameter $d = 3a_3\sqrt{c_1}/2a_2$, the potential (23) becomes

$$V = V_0 \left(1 - e^{-\sqrt{\frac{2}{3}}\chi} \right)^2 \left(\left(e^{\sqrt{\frac{2}{3}}\chi} + 1 \right) + d \left(e^{\sqrt{\frac{2}{3}}\chi} - 1 \right) \right)^2, \quad (26)$$

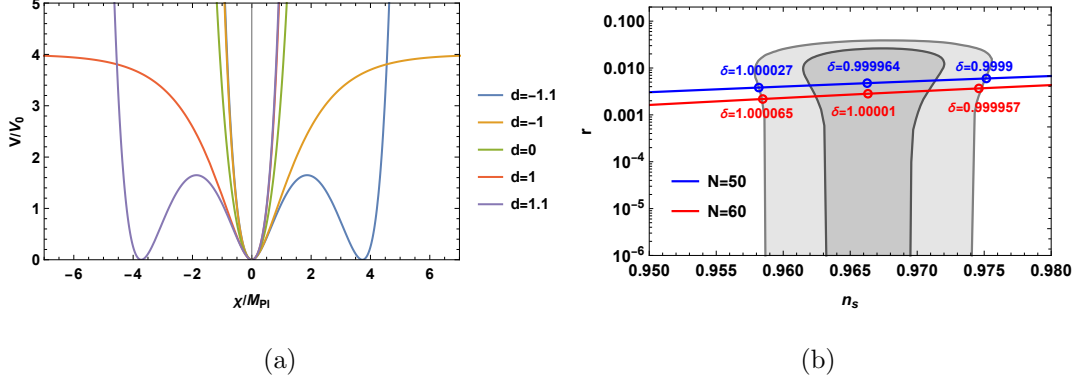


FIG. 1. Inflationary potential (a) and the r versus n_s predictions (b) for the inflaton potential in Eq. (26) with parameter $d = \pm\delta$.

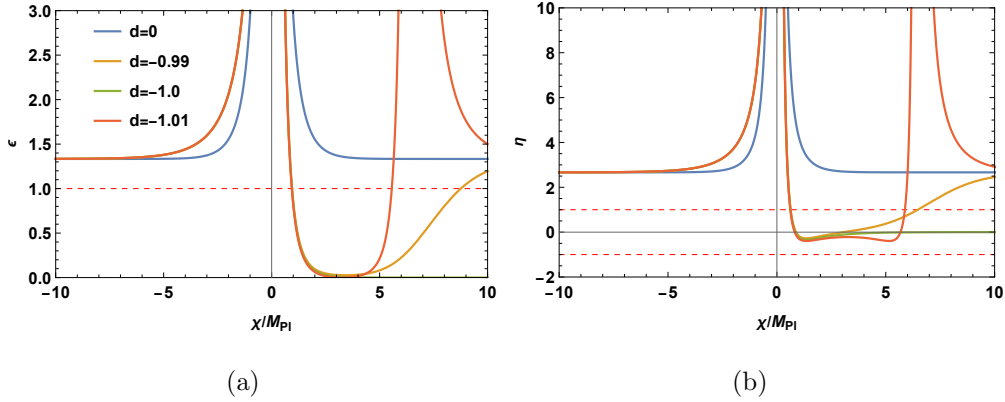


FIG. 2. The evolution of the slow-roll parameters (a) ϵ and (b) η for the inflaton potential in Eq. (26).

with $V_0 = a_2^2/12c_1$. The similar inflation in the simple Wess-Zumino model has been previously discussed by Ellis *et al.* [21]. Here for completeness, we will go through it as well. The potential with different parameter d are shown in Fig. 1(a). We note that the potential remains the same after both parameter d and field χ becoming $-d$ and $-\chi$. Therefore, we will only discuss the negative d in the following calculation.

When d is larger than -1 , there is a vacuum at $\chi = 0$. When d is smaller than -1 , there are two minima at $\chi_{m_1} = 0$ and $\chi_{m_2} = \frac{\sqrt{6}}{2} \log\left(\frac{d+1}{d-1}\right)$, and a maximum at $\chi_M = \frac{\sqrt{6}}{4} \log\left(\frac{d+1}{d-1}\right)$. From the evolution of the slow-roll parameters in Fig. 2, the possible inflationary trajectories locate in the region $[0, \infty]$ for $d \gtrsim -1$ and the region $[\chi_{m_1}, \chi_{m_2}]$ for $d \lesssim -1$. Others are ruled out due to the steep potential, and the slow-roll conditions $\epsilon, |\eta| < 1$ are not satisfied. The cosmological predictions n_s and r for the model in Eq. (26) are numerically shown in

TABLE I. The realization of T- and E-models in one modulus and three moduli models.

Cases	$V \propto W_\varphi ^2 / (c_1 - 2\varphi^2)^2$		
$a_1 = 0, 2a_2 = -3a_3\sqrt{c_1}$	$V_J \propto \frac{ \varphi(1-\sqrt{2}\varphi) ^2}{(c_1-2 \varphi ^2)^2}$	$V_E \propto (1 - e^{-\sqrt{2/3}\chi})^2$	E-model for φ^2
Cases	$V \propto W_\varphi ^2$		
$a_{1,3} = 0$	$V_J \propto \varphi ^2$	$V_E \propto \tanh^2(\chi/\sqrt{2})$	T-model for φ^2
$a_{1,2} = 0$	$V_J \propto \varphi^2 ^2$	$V_E \propto \tanh^4(\chi/\sqrt{2})$	T-model for φ^4

Fig. 1(b) and the inflationary trajectory is in the large field region $\chi \sim 5M_{Pl}$. The parameter d locates in a tiny range around ± 1 .

1. E-model realization

Particularly, when $d = -1$ or $2a_2 = -3a_3\sqrt{c_1}$, the E-model for φ^2 [11, 51] or Starobinsky inflation model [21, 24] with potential $V = V_0(1 - e^{-\sqrt{2/3}\chi})^2$ is realized, shown in Table I. The potential can be expanded as

$$V = V_0 \left(1 - 2e^{-\sqrt{2/3}\chi} + e^{-2\sqrt{2/3}\chi} \right). \quad (27)$$

The spectrum index, tensor-to-scalar ratio, and e -folding number are expressed in the form [21, 24]

$$\begin{aligned} n_s &\simeq 1 - \frac{8}{3}e^{-\sqrt{2/3}\chi} + \mathcal{O}(e^{-2\sqrt{2/3}\chi}) \\ r &\simeq \frac{64}{3}e^{-2\sqrt{2/3}\chi} + \mathcal{O}(e^{-4\sqrt{2/3}\chi}) \\ N &\simeq \frac{3}{4}e^{\sqrt{2/3}\chi} + \mathcal{O}(e^{-2\sqrt{2/3}\chi}) \end{aligned} \quad (28)$$

and

$$n_s \simeq 1 - \frac{2}{N}, \quad r \simeq \frac{12}{N^2}. \quad (29)$$

Thus, the predictions $n_s = [0.960, 0.967]$ and $r = [0.0033, 0.0048]$ for $N = [50, 60]$ are consistent with Planck and BICEP/Keck experiments [6, 7]. Similarly with the generalization in Ref. [51], replacing N_1 with αN_1 , a factor α will be added to the leading term of r and the E-models of α -attractors are achieved.

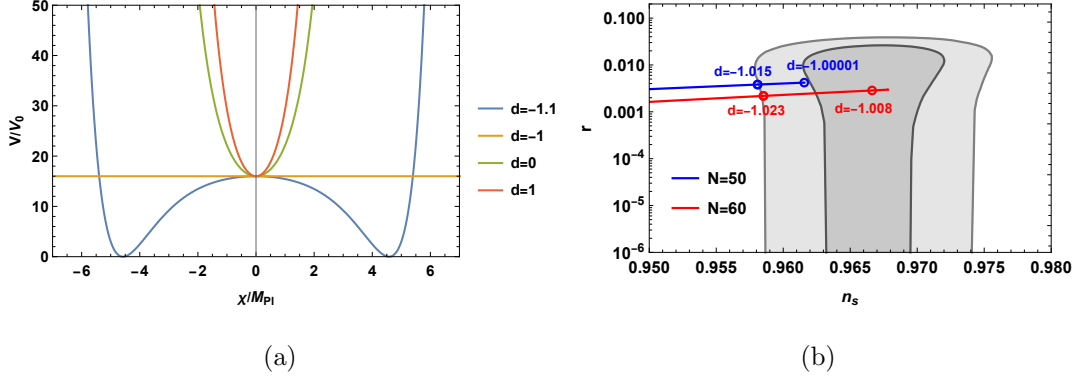


FIG. 3. Inflationary potential (a) and the r versus n_s predictions (b) for the inflaton potential in Eq. (30) with parameter $d < -1$.

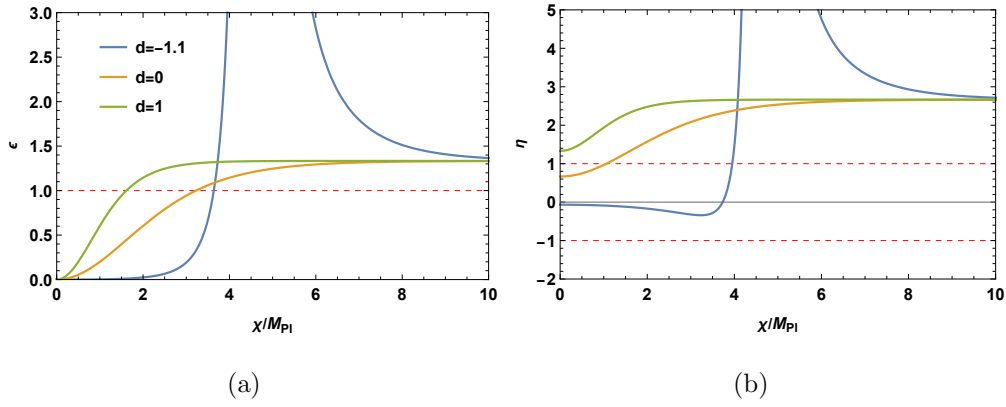


FIG. 4. The evolution of the slow-roll parameters (a) ϵ and (b) η for the inflaton potential in Eq. (30).

C. $a_2 = 0$ case

The potential becomes

$$V = V_0 e^{-2\sqrt{\frac{2}{3}}\chi} \left(\left(e^{\sqrt{\frac{2}{3}}\chi} + 1 \right)^2 + d \left(e^{\sqrt{\frac{2}{3}}\chi} - 1 \right)^2 \right)^2 \quad (30)$$

with $V_0 = a_1^2/48c_1^2$ and $d = 3a_3c_1/a_1$. The potential is an even function in terms of inflaton χ , shown in Fig. 3. So we will consider inflation in the positive field regime. When $d > -1$, there is only one minimum at $\chi_m = 0$ for the potential and the slow-roll inflation is not allowed due to $\epsilon, \eta > 1$. When $d < -1$, there are two minima at $\chi_{m1, m2} = \sqrt{3/2} \log \left(-(1 \pm \sqrt{-d})^2 / (1 + d) \right)$ and one maximum at $\chi_M = 0$ for the potential. From Fig. 4, the slow-roll parameters are $\epsilon \rightarrow 4/3$ and $\eta \rightarrow 8/3$ in the limit $\chi \rightarrow \infty$, thus inflation only happens in the region $[\phi_M, \phi_{m1}]$. The predicted observations n_s and r are also

shown in Fig. 3(b).

D. $a_3 = 0$ case

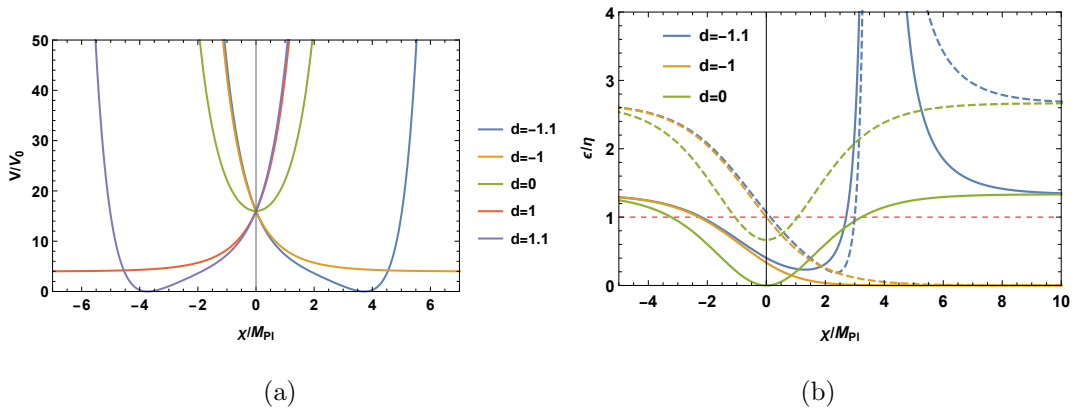


FIG. 5. Inflationary potential (a) and the evolution of the slow-roll parameters (b) for the inflaton potential in Eq. (31). The solid and dashed lines correspond to ϵ and η , respectively.

The potential becomes

$$V = V_0 \left(1 + e^{-\sqrt{\frac{2}{3}}\chi}\right)^2 \left(\left(e^{\sqrt{\frac{2}{3}}\chi} + 1\right) + d \left(e^{\sqrt{\frac{2}{3}}\chi} - 1\right)\right)^2 \quad (31)$$

with $V_0 = a_1^2/48c_1^2$ and $d = 2a_2\sqrt{c_1}/a_1$. The potential is shown in Fig. 5(a), and remains the same when both parameter d and field χ become negative. Thus, we will seek the inflation trajectory with $d \leq 0$. There is a minimum at $\chi_m = \sqrt{\frac{3}{8}} \log\left(\frac{2}{d+1} - 1\right)$ for potential with $-1 < d \leq 0$ and a minimum at $\sqrt{\frac{3}{2}} \log\left(\frac{d-1}{d+1}\right)$ with $d < -1$. From the evolution of slow-roll parameters in Fig. 5(b), we find that inflation impossibly happens for the model in Eq. (31).

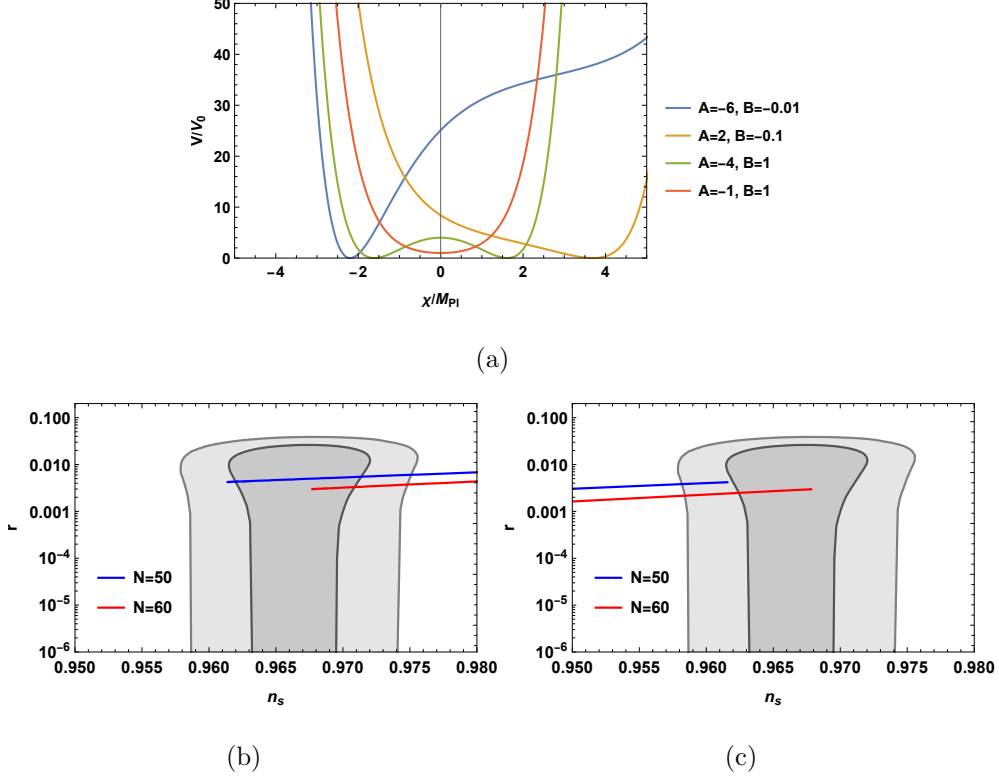


FIG. 6. Inflationary potential (a) and the r versus n_s predictions (b)-(c) for the inflaton potential in Eq. (23). Also, (b) has $B_1 < 0$, and (c) has $A_1 < 0$, $B_1 > 0$ and $A_1^2 > 4B_1$.

E. General case

To discuss the general case for the inflation model with one modulus, we will start again with the potential in Eq. (23). The slow-roll parameters are

$$\begin{aligned}
 \varepsilon(\chi) &= \frac{4 \left(B_1 e^{2\sqrt{\frac{2}{3}}\chi} - 1 \right)^2}{3 \left(1 + A_1 e^{\sqrt{\frac{2}{3}}\chi} + B_1 e^{2\sqrt{\frac{2}{3}}\chi} \right)^2}, \\
 \eta(\chi) &= \frac{4 \left(2 + A_1 e^{\sqrt{\frac{2}{3}}\chi} + A_1 B_1 e^{\sqrt{6}\chi} + 2B_1^2 e^{4\sqrt{\frac{2}{3}}\chi} \right)}{3 \left(1 + A_1 e^{\sqrt{\frac{2}{3}}\chi} + B_1 e^{2\sqrt{\frac{2}{3}}\chi} \right)^2}.
 \end{aligned} \tag{32}$$

In the limit $\chi \rightarrow \pm\infty$, $\varepsilon \rightarrow 4/3$ and $\eta \rightarrow 8/3$, inflation cannot be realized since the slow-roll conditions cannot be satisfied. By solving $V_\chi = 0$, three extreme points are obtained as

$$\begin{aligned}\chi_1 &= -\frac{1}{2}\sqrt{\frac{3}{2}}\log(B_1), \\ \chi_2 &= \sqrt{\frac{3}{2}}\log\left(-\frac{\sqrt{A_1^2 - 4B_1} + A_1}{2B_1}\right), \\ \chi_3 &= \sqrt{\frac{3}{2}}\log\left(\frac{\text{sgn}[B_1]\sqrt{A_1^2 - 4B_1} - A_1}{2B_1}\right).\end{aligned}\tag{33}$$

The potential with different parameters is shown in Fig. 6(a). When $B_1 < 0$, there is only one minimum for the potential at $\chi_m = \chi_3$, and the CMB predictions are shown in Fig. 6(b). The spectral index n_s is increasing as $|A_1|$ decreasing or $|B_1|$ increasing. When $A_1 < 0$, $B_1 > 0$ and $A_1^2 > 4B_1$, there is a maximum at $\chi_M = \chi_1$, and two minima at $\chi_{m1,m2} = \chi_{2,3}$. Thus, the possible inflationary trajectories are from χ_M to χ_{m1} or to χ_{m2} , where the CMB predictions are shown in Fig. 6(c). As $|A_1| \gg B_1$, the potential goes back to the case with $a_2 = 0$ and the inflation gives the proper CMB observed value; while for other parameter spaces, there is only one minimum for the potential at $\chi_m = \chi_1$, i.e., $V(\chi_1) = (A_1 + 2\sqrt{B_1})^2$. To avoid the cosmological constant problem, the two parameters are related as $A_1 = -2\sqrt{B_1}$. Thus, the slow-roll parameters in Eq. (32) become

$$\begin{aligned}\varepsilon(\chi) &= \frac{4}{3}\left(\frac{1 + \sqrt{B_1}e^{\sqrt{\frac{2}{3}}\chi}}{1 - \sqrt{B_1}e^{\sqrt{\frac{2}{3}}\chi}}\right)^2 \geq \frac{4}{3}, \\ \eta(\chi) &= \frac{8}{3}\frac{\left(1 + \sqrt{B_1}e^{\sqrt{\frac{2}{3}}\chi} + B_1e^{2\sqrt{\frac{2}{3}}\chi}\right)}{\left(1 - \sqrt{B_1}e^{\sqrt{\frac{2}{3}}\chi}\right)^2} \geq \frac{8}{3}.\end{aligned}$$

If we ignore the cosmological constant problem, i.e., $A_1 \neq -2\sqrt{B_1}$, the slow-roll parameters in Eq. (32) are in the ranges of

$$0 \leq \varepsilon(\chi) < \frac{4}{3}, \quad \frac{4}{3} \leq \eta(\chi) < \frac{8}{3}.$$

The slow-roll conditions are violated due to the steep slope. We also show the evolution of slow-roll parameters for models with $A_1 = -1, B_1 = 1/4$ and $A_1 = -1, B_1 = 50$ in Fig. 7.

V. TWO MODULI INFLATIONARY MODEL

In this section, we consider the no-scale inflation model realized via the orbifold compactification of M-theory on T^6/Z_{12} by keeping singlets under $SU(2) \times U(1)$ symmetry, and

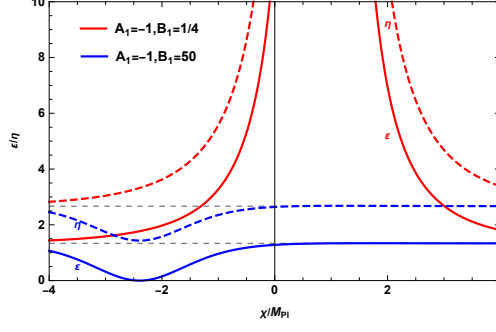


FIG. 7. The evolution of the slow-roll parameters. Solid and dashed lines are corresponding to ε and η , respectively.

then the compactification on S^1/Z_2 [59], where the Kähler potential with two moduli $T_{1,2}$ and one chiral superfield φ is

$$K = -2 \log(T_1 + \bar{T}_1 - 2|\varphi|^2) - \log(T_2 + \bar{T}_2). \quad (34)$$

Here, for simplicity we neglect the irrelevant scalar fields. The scalar potential in Jordan frame is

$$V = \frac{|W_\varphi|^2}{4c_2(c_1 - 2|\varphi|^2)}. \quad (35)$$

After field transformation with $\varphi = \sqrt{c_1/2} \tanh(\chi/2)$, it becomes

$$V = V_0 \frac{1 + A_2 e^\chi + B_2 e^{2\chi}}{e^\chi (1 + e^\chi)^2}, \quad (36)$$

with $V_0 = \frac{(a_1 - 2a_2\sqrt{c_1} + 3a_3c_1)^2}{8c_1c_2}$, $A_2 = \frac{2(a_1 - 3a_3c_1)}{a_1 - 2a_2\sqrt{c_1} + 3a_3c_1}$ and $B_2 = \frac{a_1 + 2a_2\sqrt{c_1} + 3a_3c_1}{a_1 - 2a_2\sqrt{c_1} + 3a_3c_1}$.

A. $a_1 = 0$ case

The scalar potential is

$$V = V_0 \frac{(1 - e^\chi)^2 \left(1 + \frac{1+d}{1-d} e^\chi\right)^2}{e^\chi (1 + e^\chi)^2} \quad (37)$$

where $V_0 = (2a_2 - 3a_3\sqrt{c_1})^2 / 8c_2$ and $d = 3a_3\sqrt{c_1} / 2a_2$. From Fig. 8, the potential remains the same after both parameter d and field χ become negative. Therefore, in the following we will only discuss inflation with $d \geq 0$.

When $d > \sqrt{27/32}$, the potential has three extreme points: $\chi_{m1} < \chi_M < \chi_{m2} = 0$. There are four trajectories for inflation: on the left side of the minimum χ_{m1} , from the maximum

χ_M to its minima $\chi_{m1,m2}$ and on the right sides of the minimum χ_{m2} . However, slow-roll inflation cannot occur on the left side of χ_{m1} and on the right side of χ_{m2} , since the slow-roll parameters $\varepsilon \rightarrow 1/2$ and $\eta \rightarrow 1$ when $|\chi| > 5M_{\text{Pl}}$, as shown in Fig. 9. Moreover, we find that inflation cannot end on the trajectory from χ_M to χ_{m1} , and slow-roll inflation is not permitted from χ_M to χ_{m2} because of $\eta(\chi_M)$ greater than 1.

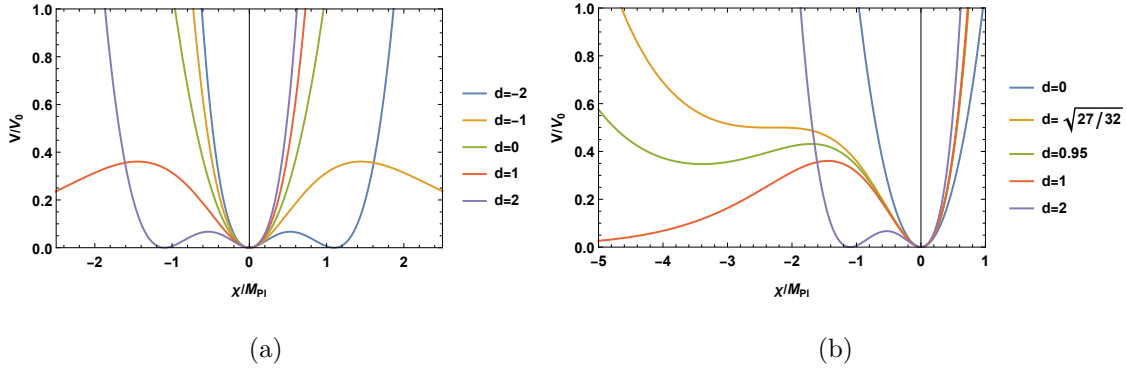


FIG. 8. The inflaton potential in Eq. (37).

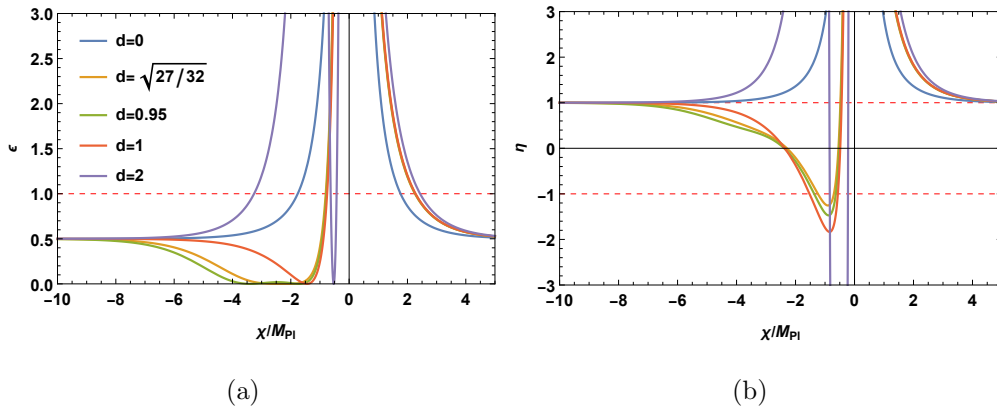


FIG. 9. The evolution of the slow-roll parameters (a) ε and (b) η for the inflaton potential in Eq. (37).

When $0 \leq d \leq \sqrt{27/32}$, the potential has a minimum at χ_{m2} and the potential has an inflection point when $d = \sqrt{27/32}$. Here, we will discuss the impossibility for the inflation along the right side of the minimum. For the sake of convenience, we choose $d = 0$, where the potential becomes

$$V = \frac{2a_2^2}{c_2} \sinh^2 \left(\frac{\chi}{2} \right). \quad (38)$$

In this case, the slow-roll parameters are

$$\begin{aligned}\varepsilon(\chi) &= \frac{1}{2} \coth^2\left(\frac{\chi}{2}\right), \\ \eta(\chi) &= \frac{1}{2} \cosh(\chi) \operatorname{csch}^2\left(\frac{\chi}{2}\right).\end{aligned}\tag{39}$$

The parameter η is larger than 1 on the whole trajectory. Therefore, slow-roll inflation cannot be obtained when $d = 0$. Similarly, inflation from the right side of $\chi_{m2} = 0$ for all d and from the left side of χ_{m1} for $d > \sqrt{27/32}$ is not allowable as well.

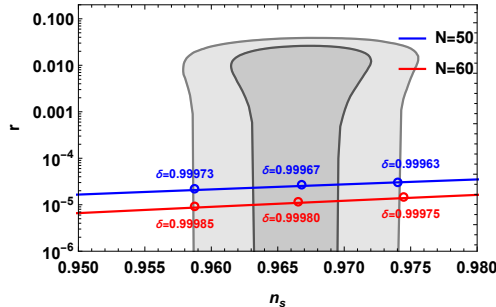


FIG. 10. The r versus n_s predictions for the inflaton potential in Eq. (37) with parameter $d = \sqrt{27/32}\delta$.

Thus, the feasible inflationary trajectory is on the left side of $\chi_{m2} = 0$ for $0 < d \leq \sqrt{27/32}$. Similar to the Starobinsky-like E-model with one modulus, the predicted r that satisfy the experimental limits are obtained from a tiny region for the parameter $d \lesssim \sqrt{27/32}$. The results are shown in Fig. 10, where we also show triple-pack benchmark points corresponding to the central and 2σ bound values for observed n_s . Thus, the spectrum index is increasing as the parameter d is decreasing. From the numerical calculations, one notes that inflation initials at $\chi_* \simeq -2.26M_{\text{Pl}}$, the higher order term $\left(\frac{1+d}{1-d}e^x\right)^2$ of the numerator in Eq.(37) is not small and cannot be ignored. When $d = \sqrt{27/32}$, the tensor-to-scalar ratio r and e -folding number are approximate to be

$$\begin{aligned}r &\simeq \frac{8(5 - 3(8\sqrt{6} + 13)e^x + 3(32\sqrt{6} + 77)e^{2x})^2}{(5 + (24\sqrt{6} + 59)e^x)^2} \\ N &\simeq \frac{824 - 336\sqrt{6}}{(11\sqrt{6} - 24)e^x - 103\sqrt{6} + 252}\end{aligned}$$

and

$$r \simeq \frac{8192(49 - 20\sqrt{6})}{N^4} \simeq \frac{83.60}{N^4}\tag{40}$$

For $N = 50 - 60$, the predicted r is about 10^{-5} and consistent with numerical calculations.

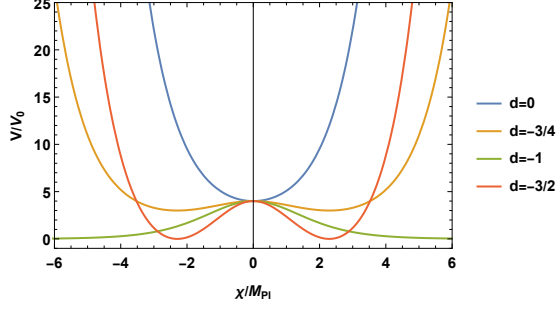


FIG. 11. Inflaton potential in Eq. (41).

B. $a_2 = 0$ case

The scalar potential becomes

$$V = V_0 \frac{((e^x + 1)^2 + d(e^x - 1)^2)^2}{e^{-x}(e^x + 1)^2} \quad (41)$$

with $V_0 = a_1^2/(8c_1c_2)$ and $d = 3a_3c_1/a_1$. It is an even function in terms of χ . Thus, for simplicity, we will study inflation in the positive region $\chi > 0$, as shown in Fig. 11. There is a minimum and maximum at $\chi = 0$ for the potential with $d \geq -1/2$ and $d = -1$, respectively. Also, there is a maximum at $\chi_M = 0$ and two minima at $\chi_m = \log\left(-\left(1 + 3d \pm 2\sqrt{d(2d+1)}\right)/(d+1)\right)$ and $\chi_m = \log\left(-\left(1 - d \pm 2\sqrt{-d}\right)/(d+1)\right)$ respectively for $-1 < d < -1/2$ and $d < -1$. However, the slow-roll inflation cannot end. To understand this behavior, we choose $d = -1$, and the corresponding slow-roll parameters in terms of the field χ are

$$\varepsilon(\chi) = \frac{1}{2} - \frac{2e^\chi}{(e^\chi + 1)^2}, \quad \eta(\chi) = 1 - \frac{6e^\chi}{(e^\chi + 1)^2}. \quad (42)$$

Thus, we have $\varepsilon(0) = 0$, $\eta(0) = -1/2$. For $\chi > 0$, we have $0 < \varepsilon < 1/2$, $-1/2 < \eta < 1$, and $\eta \rightarrow 1$ as $\chi \rightarrow \infty$. Thus, we cannot exit the slow-roll inflation.

C. $a_3 = 0$ case

The scalar potential with $a_3 = 0$ becomes

$$V = V_0 e^{-x} ((e^x + 1) + d(e^x - 1))^2 \quad (43)$$

where $V_0 = a_1^2/8c_1c_2$ and $d = 2a_2\sqrt{c_1}/a_1$. Because the potential is invariant as $d \rightarrow -d$ and $\chi \rightarrow -\chi$ (see Fig. 12), we only need to study the cosmological predictions with $d \geq 0$.

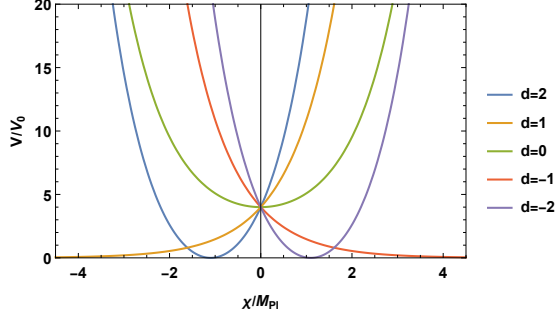


FIG. 12. Inflaton potential in Eq. (43).

There is a minimum at $\chi_m = \log(|1 - d|/(1 + d))$. Note that $V(\chi_m)$ is larger than 0 with $d < 1$, we have the cosmological constant problem. However, it still does not have slow-roll inflation with $d \geq 1$. The slow-roll parameters are

$$\varepsilon(\chi) = \frac{(e^\chi + \xi)^2}{2(e^\chi - \xi)^2}, \quad \eta(\chi) = 1 + \frac{2\xi e^\chi}{(e^\chi - \xi)^2} \quad (44)$$

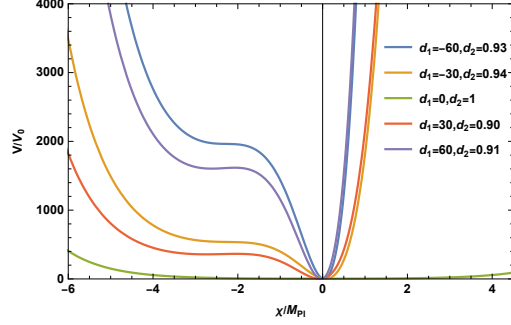
with $\xi = (d - 1)/(d + 1)$. For $d \geq 1$, we obtain $\eta \geq 1$, and thus the slow-roll conditions cannot be satisfied.

D. General case

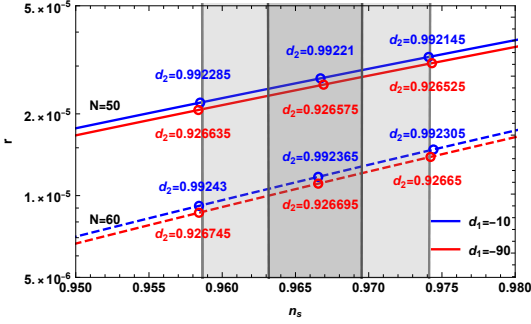
Now, we discuss the general case whose inflaton potential is

$$V = V_0 \frac{((e^\chi + 1)^2 + d_1(e^\chi - 1)((e^\chi + 1) + d_2(e^\chi - 1)))^2}{e^\chi(e^\chi + 1)^2} \quad (45)$$

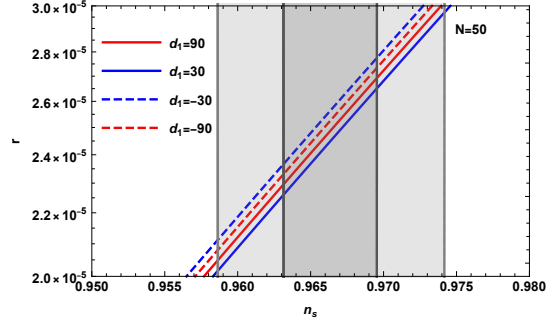
with $V_0 = a_1^2/8c_1c_2$, $d_1 = 2a_2\sqrt{c_1}/a_1$ and $d_2 = 3a_3\sqrt{c_1}/2a_2$. The potential remains the same after both parameters d_1, d_2 and field χ become negative. Thus, we will only discuss inflation with $d_2 \geq 0$. The potential and r versus n_s predictions are shown in Fig. 13. The possible inflation is along the flat trajectory $\chi < 0$. Similar to the $a_1 = 0$ case, the inflation is sensitive to the parameter d_2 and the benchmark points corresponding to the central and 2σ bound values for observation n_s are also shown in Fig. 13(b). The solid and dashed lines are corresponding to $N = 50$ and $N = 60$, respectively. From the numerical results, we know that the spectrum index increases as the parameter d_2 decreases. Moreover, the tensor-to-scalar ratio r predicted from models with $d_1 < 0$ is larger than that with $d_1 > 0$. We plot r versus n_s for models with $d_1 = \pm 30, \pm 90$ in Fig. 13(c).



(a)



(b)



(c)

FIG. 13. The r versus n_s predictions (b),(c) for the inflaton potential (a) in Eq. (45).

VI. THREE MODULI INFLATIONARY MODEL

In this section, we consider no-scale inflation realized by the orbifold compactifications of M-theory on T^6/Z_{12} as well as S^1/Z_2 [59], which has three moduli and the Kähler potential is given by Eq. (10) with $N_1 = N_2 = N_3 = 1$. Stabilizing the moduli with $T_i = \bar{T}_i = c_i/2$, the scalar potential along the real part of field φ is given by

$$V = \frac{|W_\varphi|^2}{2c_2c_3}. \quad (46)$$

The three moduli inflationary model is similar to that with the global supersymmetry, and has a non-negative scalar potential, but the Kähler potential is different. Redefining the canonical field χ with $\varphi = \sqrt{c_1/2} \tanh(\chi/\sqrt{2})$, the potential becomes

$$V = V_0 \frac{\left(1 + A_3 e^{\sqrt{2}\chi} + B_3 e^{2\sqrt{2}\chi}\right)^2}{\left(1 + e^{\sqrt{2}\chi}\right)^4} \quad (47)$$

with $V_0 = \frac{(a_1 - 2a_2\sqrt{c_1} + 3a_3c_1)^2}{c_2c_3}$, $A_3 = \frac{2(a_1 - 3a_3c_1)}{a_1 - 2a_2\sqrt{c_1} + 3a_3c_1}$, and $B_3 = \frac{a_1 + 2a_2\sqrt{c_1} + 3a_3c_1}{a_1 - 2a_2\sqrt{c_1} + 3a_3c_1}$.

A. T-model realization: $a_{1,3} = 0$ and $a_{1,2} = 0$ cases

When $a_{1,3} = 0$, the inflation model in Eq. (46) reduces to $V \propto \varphi^2$. We know that the chaotic inflation [67, 68] predicts

$$n_s \simeq 1 - \frac{2}{N}, \quad r \simeq \frac{8}{N}, \quad (48)$$

which will give a larger $r \sim 0.14$ for $N \sim 55$ and the inflation with a quadratic potential is ruled out by the Planck and BICEP/Keck experiments [6, 7]. After field transformation, the T-model [51] for the φ^2 inflation model is achieved with potential as

$$V = V_0 \tanh^2 \left(\frac{\chi}{\sqrt{2}} \right). \quad (49)$$

Similar, the T-model [51] for φ^4 is realized with $a_{1,2} = 0$ and the potential is given by $V = V_0 \tanh^4 (\chi/\sqrt{2})$. We list the realization of the T-model in the three moduli model in Table I. If the factor N_1 is generalized to αN_1 , the T-model of the α -attractor can be obtained.

For the T-model for φ^{2n} , the slow-roll parameters are

$$\begin{aligned} \varepsilon &= 4n^2 \operatorname{csch}^2 \left(\sqrt{2}\chi \right), \\ \eta &= 4n \left(2n - \cosh \left(\sqrt{2}\chi \right) \right) \operatorname{csch}^2 \left(\sqrt{2}\chi \right). \end{aligned} \quad (50)$$

The inflation ends at $\chi_e = \sinh^{-1}(2n)/\sqrt{2}$ with $\varepsilon = 1$. Then the e -folding number can be rewritten in terms of the inflaton at horizon crossing χ_*

$$\begin{aligned} N &= \frac{1}{4n} \cosh \left(\sqrt{2}\chi \right) \Big|_{\chi_e}^{\chi_*} \\ &= \frac{1}{4n} \left(\cosh \left(\sqrt{2}\chi_* \right) - \sqrt{4n^2 + 1} \right) \end{aligned} \quad (51)$$

The cosmological predictions are given by

$$\begin{aligned} n_s &= 1 - \frac{2 \left(n + \sqrt{4n^2 + 1} + 4nN \right)}{n + 2N\sqrt{4n^2 + 1} + 4nN^2} \\ r &= \frac{16n}{n + 2N\sqrt{4n^2 + 1} + 4nN^2} \end{aligned} \quad (52)$$

Comparing with Eq. (48), the spectral index changes a little, whereas the tensor-to-scalar ratio is effectively suppressed by the factor $4/N^2$: $n_s = 0.9602$, $r = 0.0016$ for $N = 50$, and $n_s = 0.9668$, $r = 0.0011$ for $N = 60$.

B. $a_1 = 0$ case

The effective potential of scalar field φ is

$$V = \frac{4}{c_2 c_3} \left| \sqrt{2} a_2 \varphi + 3 a_3 \varphi^2 \right|^2, \quad (53)$$

and can be rewritten as a three-term polynomial inflation model $V = V_0 |\phi + \alpha \phi^2|^2$ which predicts a large tensor-to-scalar ratio $r \sim [0.025, 0.249]$ [69] and the parameter space is partially ruled out by the latest limits. However, the field φ is noncanonical in the no-scale SUGRA models. In the following discussion, one will find that tensor-to-scalar ratio r is suppressed by $1/N^2$ rather than $1/N$.

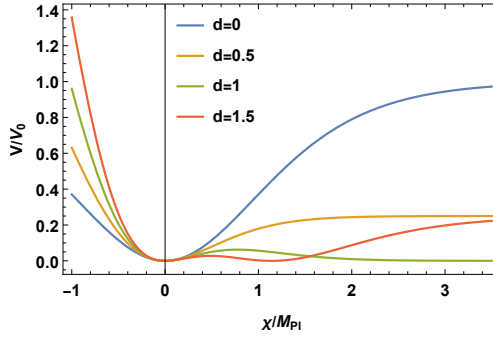


FIG. 14. Inflaton potential in Eq. (54).

Using the field transformation, the potential with canonical field χ can be rewritten in the general form Eq. (47) with $V_0 = \frac{(2a_2\sqrt{c_1}-3a_3c_1)^2}{c_2c_3}$, $A_3 = \frac{6a_3c_1}{2a_2\sqrt{c_1}-3a_3c_1}$, $B_3 = -\frac{2a_2\sqrt{c_1}+3a_3c_1}{2a_2\sqrt{c_1}-3a_3c_1}$. The two parameters A_3 and B_3 are interrelated, $A_3 + B_3 = -1$. After defining a new parameter $d = -3a_3\sqrt{c_1}/2a_2$, they become $A_3 = -2d/(d+1)$ and $B_3 = d-1/(d+1)$. The potential can be rewritten with two parameters V_0 and d as follows:

$$V = V_0 \frac{\left(d \left(e^{\sqrt{2}\chi} - 1 \right)^2 - e^{2\sqrt{2}\chi} + 1 \right)^2}{\left(1 + e^{\sqrt{2}\chi} \right)^4}. \quad (54)$$

The parameter $V_0 = 4a_2^2c_1/c_2c_3$ can be fixed by the power spectrum $A_s = 2.10 \times 10^{-9}$ [6] at horizon crossing. One can find that the potential $V(-d, -\chi)$ equals to $V(d, \chi)$, which indicates that the negative trajectory $\chi < 0$ with $d < 0$ will give the same observations with positive trajectory $\chi > 0$ with $d > 0$, and vice versa. For convenience, we study the inflation by setting $d > 0$. Inflation with $d = 0$ was discussed in the previous subsection.

The potential in terms of inflaton field χ with different parameter d are shown in Fig. 14. There is a minimum at $\chi = 0$, and the inflation will occur on the negative branch R_1 ($\chi < \chi_m$ region). Since the steep trajectory in the region of $\chi < 0$ weakly depends on the parameter d , the potential goes back to that in the previous $a_{1,3} = 0$ case (T-model) and the predictions are $n_s \simeq 0.9602$ and $r \simeq 0.0016$ for $N = 50$, as well as $n_s \simeq 0.9667$ and $r \simeq 0.0011$ for $N = 60$. Next, we will study inflation on the positive field branch $\chi > 0$. Similar to the $a_{1,3} = 0$ case, the potential with $d < 1/2$ only has one minimum at $\chi = 0$. The inflation can occur at both branches $\chi > 0$ and $\chi < 0$, however, the two inflation trajectories are not symmetric. When the inflation occurs at the positive branch $\chi > 0$, n_s and r are very sensitive to d . The numerical results are shown in Fig. 15 and n_s has a maximum when $d = 0.465$: $n_s = 0.9636(0.9697)$ for e -folds $N = 50(60)$. When $1/2 < d \leq 1$, the potential has a minimum at $\chi_m = 0$ and a maximum at $\chi_M = \sqrt{2} \tanh^{-1}(1/2d)$. There are three possible inflation trajectories, labeled as R_1 ($\chi < \chi_m$ region), R_2 ($\chi_m < \chi < \chi_M$ region), and R_3 ($\chi > \chi_M$ region). The parameter is restricted to a range $0.5 < d < 0.55$ for the R_2 trajectory due to small n_s and lack of e -folds. The scalar spectral index n_s decreases as d is increasing and the numerical results are shown in Fig. 16(a). The last trajectory R_3 is ruled out since the potential is too flat where the inflation either cannot end or cannot last long enough. When $d > 1$, the potential has two minima at $\chi_{m_1} = 0$ and $\chi_{m_2} = \sqrt{2} \tanh^{-1}(1/d)$ and one maximum at $\chi_M = \sqrt{2} \tanh^{-1}(1/2d)$. Thus, there are four possible trajectories, labeled as R_1 ($\chi < \chi_m$ region), R_2 ($\chi_{m_1} < \chi < \chi_M$ region), R_3 ($\chi_M < \chi < \chi_{m_2}$ region), and R_4 ($\chi > \chi_{m_2}$ region). As discussed above, the inflation in R_2 and R_3 is forbidden since the e -folding numbers are not enough. The inflation on R_4 is similar to that on negative branch R_1 and the results are shown in Fig. 16(b). At last, the above results are summarized in Fig. 17.

As discussed above, $e^{-\sqrt{2}\chi^*}$ is small as the mode crossing the horizon, then potential (54) is expanded up to the leading order in $e^{-2b\chi}$ as

$$V \propto (1 - ae^{-2b\chi} + \mathcal{O}(e^{-4b\chi})) \quad (55)$$

where $a = 4(1 - 2d)/(1 - d)$ and $b = 1/\sqrt{2}$. The spectrum index, tensor-to-scalar ratio, and

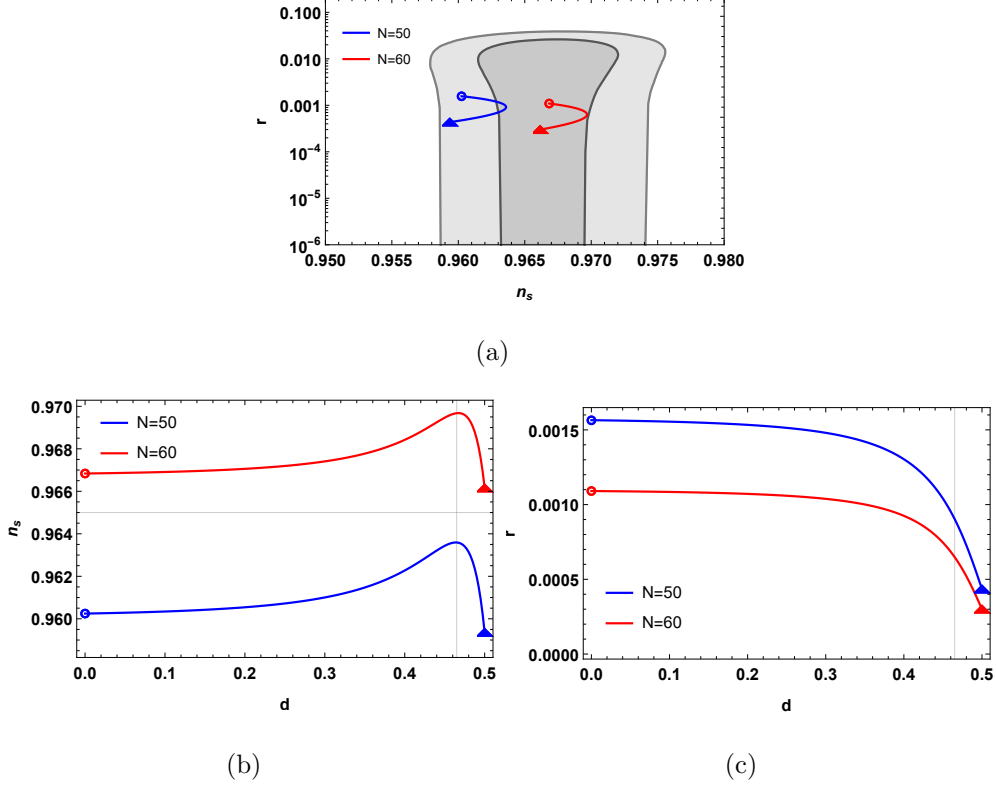


FIG. 15. (a) The r versus n_s predictions for the inflaton potential in Eq. (54) with $d \leq 1/2$; (b) n_s versus the parameter d , and (c) r versus the parameter d . The circles and triangles correspond to $d = 0$ (T-model for φ^2) and $d = 1/2$, respectively.

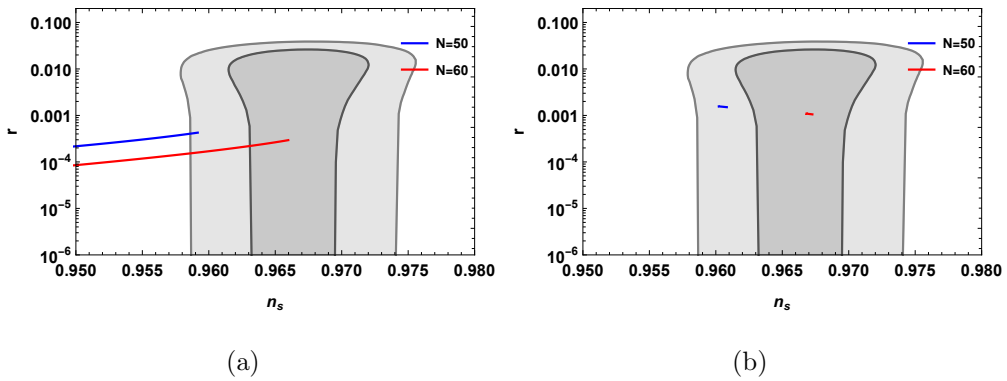


FIG. 16. The r versus n_s predictions for the inflaton potential in Eq. (54) with (a) $1/2 < d \leq 1$ and (b) $d > 1$.

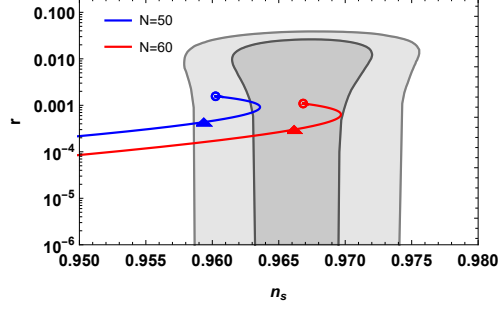


FIG. 17. The r versus n_s predictions for the inflaton potential in Eq. (54). The circles and triangles correspond to $d = 0$ (T-model for φ^2) and $d = 1/2$, respectively.

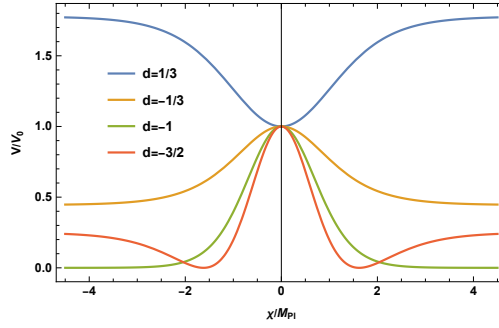


FIG. 18. Inflaton potential in Eq. (60).

e -folding number are

$$n_s \simeq 1 - 8ab^2 e^{-2b\chi} + \mathcal{O}(e^{-4b\chi}) \quad (56)$$

$$r \simeq 32a^2 b^2 e^{-4b\chi} + \mathcal{O}(e^{-8b\chi}) \quad (57)$$

$$N \simeq \frac{e^{2b\chi}}{4ab^2} + \mathcal{O}(e^{-4b\chi}) \quad (58)$$

and

$$n_s \simeq 1 - \frac{2}{N}, \quad r \simeq \frac{2}{b^2 N^2}. \quad (59)$$

Thus, the predictions $n_s = [0.960, 0.967]$ and $r = [0.0016, 0.0011]$ for $N = [50, 60]$ are consistent with the Planck 2018 results [6].

C. $a_2 = 0$ case

When $a_2 = 0$, the potential with canonical field χ can be rewritten as

$$V = V_0 \left(1 + d \tanh^2 \left(\frac{\chi}{\sqrt{2}} \right) \right)^2 \quad (60)$$

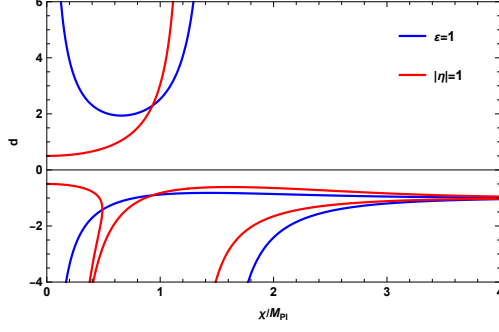


FIG. 19. The parameter d with respect to inflaton χ/M_{Pl} .

with $V_0 = a_1^2/c_2c_3$ and $d = 3a_3c_1/a_1$, and we show the potential with different d in Fig. 18. From the plots, one notes that the positive and negative branches are symmetric, and here we will only discuss the inflation for the positive branch. Thus, we need to find the possible parameter space of d for inflation. The slow-roll parameters are given by the following analytic form

$$\varepsilon = \frac{16d^2 \tanh^2(b\chi)}{((d+1) \cosh(2b\chi) - d + 1)^2},$$

$$\eta = \frac{d(1 - 2\xi_1 \cosh(2b\chi) + \xi_2 \cosh(4b\chi)) \operatorname{sech}^6(b\chi)}{6(3d-1)(d \tanh^2(b\chi) + 1)^2}.$$

with $\xi_1 = (5d+1)/(9d-3)$ and $\xi_2 = (d+1)/(9d-3)$. Solving the equations of $\varepsilon = 1$ and $|\eta| = 1$, we get

$$\varepsilon = 1 \rightarrow d_1 = \frac{2 \cosh^2(b\chi) \coth(b\chi)}{4 \mp \sinh(2b\chi)},$$

$$|\eta| = 1 \rightarrow d_2 = \begin{cases} \frac{(\Delta_1 \pm \Delta_2) \coth^2(b\chi)}{\cosh(4b\chi) + 16 \cosh(2b\chi) - 65} \\ \frac{(\Delta_3 \pm \Delta_4) \coth^2(b\chi)}{\cosh(4b\chi) - 16 \cosh(2b\chi) + 63} \end{cases}, \quad (61)$$

where $\Delta_1 = 8\sqrt{\cosh(4b\chi) - 4 \cosh(2b\chi) + 4}$, $\Delta_2 = \cosh(4b\chi) + 8 \cosh(2b\chi) - 17$, $\Delta_3 = 8\sqrt{5 - 4 \cosh(2b\chi)}$, and $\Delta_4 = \cosh(4b\chi) - 8 \cosh(2b\chi) + 15$. Due to the complicated formula, we plot d versus χ/M_{Pl} in Fig. 19 and find that the inflation will occur at the regime $|d| > 1/2$ since inflaton will go down to the vacuum of potential without truncation when $|d| < 1/2$. The evolution of slow-roll parameters in terms of inflaton field are shown in Fig. 20.

When $d > 1/2$, there is a minimum for the potential at $\chi_m = 0$, and the gradient increases as d increases, which indicates that inflation can be truncated only with large d . Based on the evolution of slow-roll parameters from Fig. 20, one can find that inflation will end if

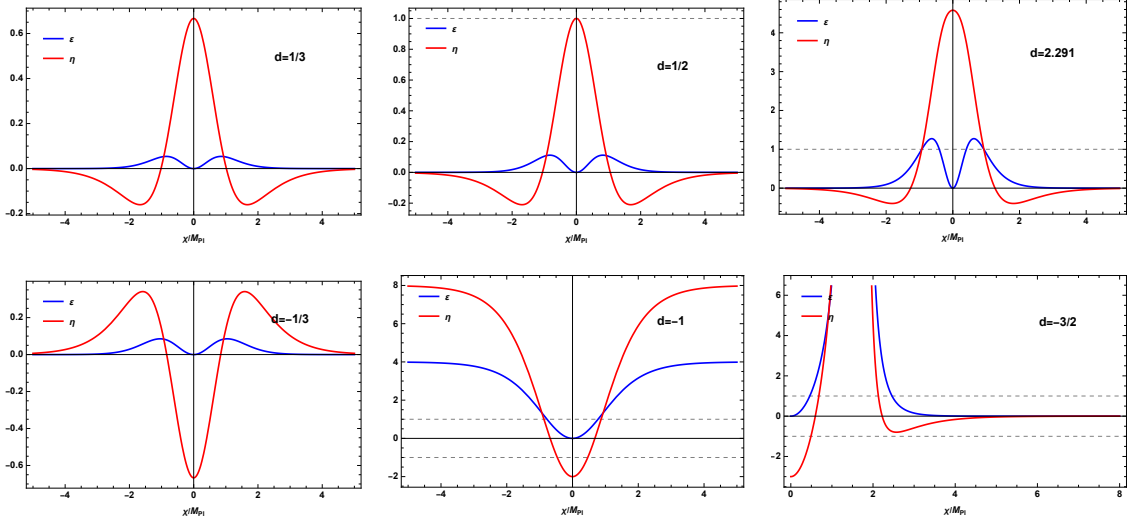


FIG. 20. The evolutions of the slow-roll parameters ε , η for the inflaton potential in Eq. (60) .

the condition $\varepsilon = 1$ is satisfied when $d > 1.937$, whereas inflation will first end at $\eta = 1$ until $d > 2.291$. The predictions n_s and r for $N = 50$ and 60 are shown with dashed lines in Fig. 21. As d is rising, the scalar spectral index n_s is increasing. In the limit $d \rightarrow \infty$, the constant term 1 can be ignored in the potential (60) and then the α -attractor T-model for ϕ^4 [51] can be achieved. As the parameter d locates in the range $-1 < d < -1/2$, there is only a maximum for the potential at $\chi = 0$. However, slow-roll inflation cannot happen due to the large $|\eta|$. While $d < -1$, there is a maximum at $\chi = 0$ and two minima at $\chi_m = \pm\sqrt{2}\tanh^{-1}\left(\sqrt{1/|d|}\right)$. From the evolution of the slow-roll parameters, inflation only occurs at the region $\chi > \chi_m$ and the predictions are shown with solid lines in Fig. 21. The spectral index n_s and the tensor-to-scalar ratio r slightly depend on the parameter d , and n_s improves when the parameter d goes from $-\infty$ to -1 . In the limit $d \rightarrow -1$, the inflaton $\chi_* \sim 6M_{\text{Pl}}$ and $e^{-\sqrt{2}\chi_*}$ is small when the pivot scale leaves the horizon, so the potential (60) can be expanded as

$$V \simeq V_0(1+d)^2 \left(1 - \frac{4d}{1+d}e^{-\sqrt{2}\chi}\right)^2. \quad (62)$$

The E-model [11, 51] is carried out and the predicted observations are

$$n_s \simeq 1 - \frac{8(4N+1)}{(1-4N)^2}, \quad r \simeq \frac{64}{(1-4N)^2}. \quad (63)$$

The numerical results of the predictions for T- and E-models are also shown as circles and triangles in Fig. 21, respectively. One notes that the zeroth and first order in $e^{-\sqrt{2}\chi}$

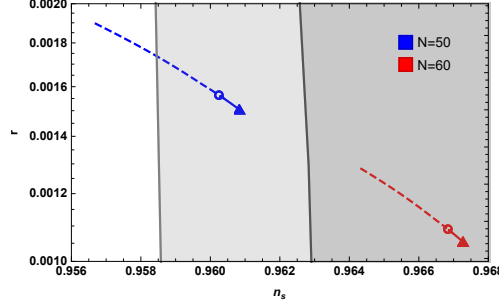


FIG. 21. The CMB predictions for the model in Eq. (60). The circles and triangles are corresponding to T- and E-model, respectively.

TABLE II. The possible parameter space for d .

Condition	d	
	$a_2 = 0$ case	$a_3 = 0$ case
$\varepsilon = 1$	$[-\infty, -1) \cup [2.2911, \infty]$	$[-\infty, -1] \cup [1, \infty]$
$ \eta = 1$	$[0.5, 2.2911]$	$[-1, -0.5774] \cup [0.5774, 1]$
No truncation	$[-0.5, 0.5]$	$[-0.5774, 0.5774]$
No slow-roll	$[-1, -0.5]$	

expansion for the potential of T- and E-models are identical, however, the precise predictions are different due to the distinction at the higher orders when $\sqrt{2}\chi \simeq \mathcal{O}(1)$. We conclude the possible parameter space for d in Table II.

D. $a_3 = 0$ case

The inflaton potential in terms of canonical field χ is

$$V = V_0 \left(1 + d \tanh \left(\frac{\chi}{\sqrt{2}} \right) \right)^2, \quad (64)$$

with $V_0 = a_1^2/c_2c_3$ and $d = 2a_2\sqrt{c_1}/a_1$. The inflaton potential is shown in Fig. 22(a), and we will only consider inflation with $d > 0$, given the equivalent potential under the exchange $(d, \chi) \leftrightarrow (-d, -\chi)$. The slow-roll parameters are

$$\begin{aligned} \varepsilon &= \frac{d^2 \operatorname{sech}^4(b\chi)}{(1 + d \tanh(b\chi))^2}, \\ \eta &= \frac{d \operatorname{sech}^4(b\chi) (2d - d \cosh(2b\chi) - \sinh(2b\chi))}{(1 + d \tanh(b\chi))^2}. \end{aligned} \quad (65)$$

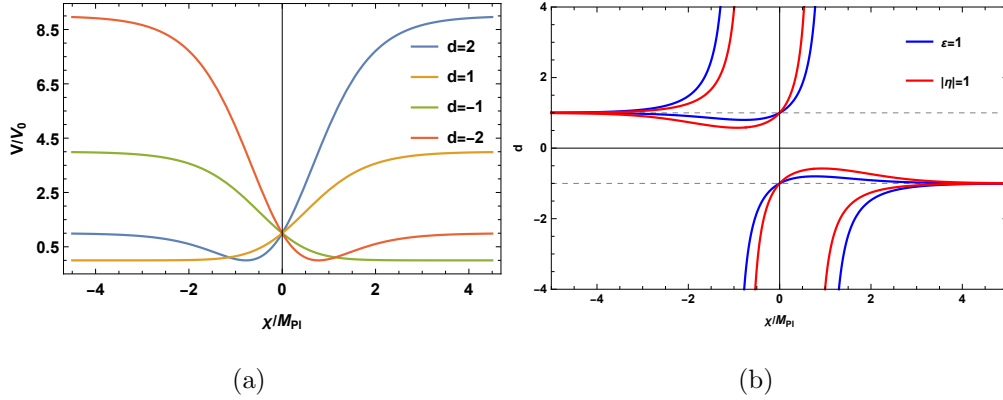


FIG. 22. Inflation potential in Eq. (64) (a) and its possible parameter space for d (b).

Under the slow-roll conditions, the solutions for the parameter d with respect to inflaton χ are

$$\begin{aligned} \epsilon = 1 &\rightarrow d_1 = \frac{2 \cosh^2(b\chi)}{\sinh(2b\chi) \pm 2}, \\ |\eta| = 1 &\rightarrow d_2 = \begin{cases} -\frac{2 \cosh(b\chi)(\Delta_1 \pm \Delta_2)}{8 \cosh(2b\chi) + \cosh(4b\chi) - 17} \\ \frac{-2i \cosh(b\chi) \pm \sinh(2b\chi)}{2i \sinh(b\chi) \pm (3 - \cosh(2b\chi))} \end{cases}, \end{aligned} \quad (66)$$

where $\Delta_1 = 5 \sinh(b\chi) + \sinh(3b\chi)$, and $\Delta_2 = 4\sqrt{\cosh(2b\chi)}$. From Figs. 22(b) and 23, one can find that it is hard to end inflation when $|d| < 0.5774$ due to the too flattened potential. When $d \in [0.5774, 1]$, inflation ends first as the condition $|\eta| = 1$ is satisfied, even the condition $\epsilon = 1$ has a solution as $d > 0.8$. There is no extreme point for the potential and the inflaton rolls from the positive to the negative region. The numerical predictions are given by dotted lines in Fig. 24 and the spectral index n_s increases with d increasing. With other $d \geq 1$, there is a minimum for the potential and inflation can happen in the two trajectories, right and left sides of the minimum. In both branches, inflation ends when the condition $\epsilon = 1$ is satisfied. The predicted n_s and r for inflation on the right and left trajectories are given by solid and dashed lines, respectively, in Fig. 24. As parameter d is increasing, the index n_s on the right trajectory increases, while n_s on the left trajectory decreases. The possible choices for parameter d are also shown in Table II.

As discussed before, in the limit $d \rightarrow \infty$, the constant term 1 can be ignored and the potential in Eq. (64) returns to $\tanh^2(\chi/\sqrt{2})$, which is identical to the potential of the T-model for φ^2 [51]. In this way, the left and right trajectories are symmetric and give the same cosmological predictions, which makes the connection of solid lines and dashed lines in

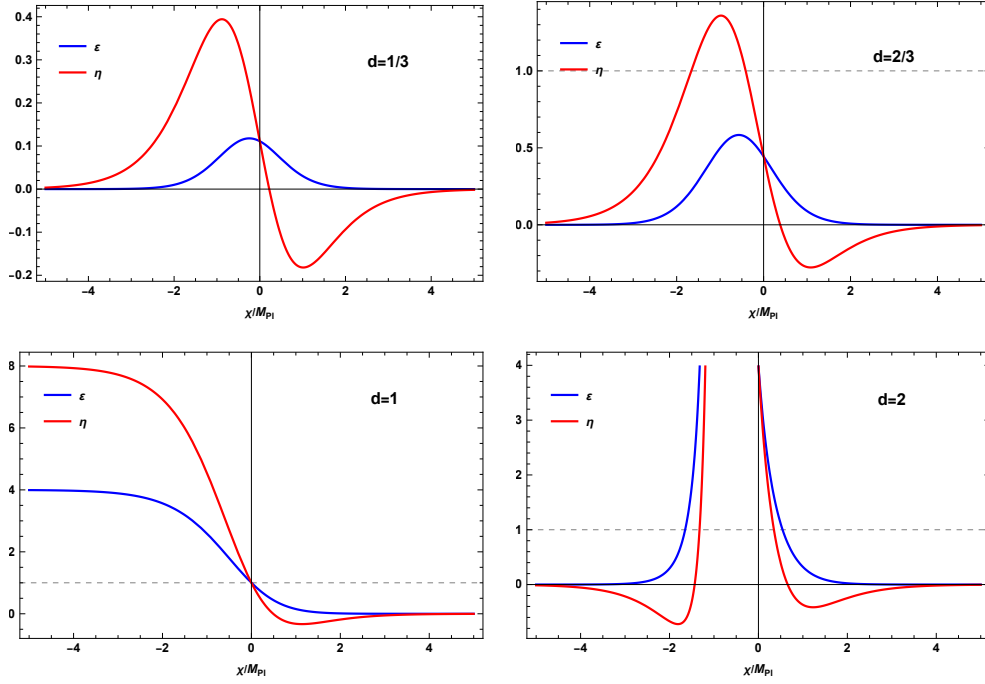


FIG. 23. The evolution of the slow-roll parameters ε and η .

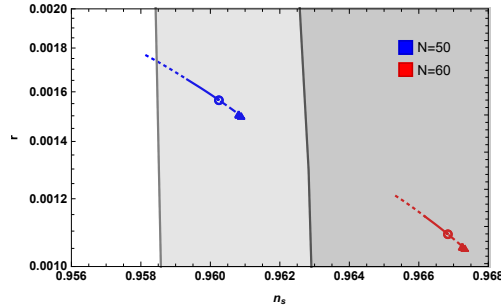


FIG. 24. The r versus n_s predictions for the inflaton potential in Eq. (64). The circles and triangles correspond to T- and E-models, respectively.

Fig. 24. While in the limit $d \rightarrow 1$, the E-model can be realized by expanding the potential in Eq. (64) on the left trajectory as $V \propto \left(1 - \frac{2d}{1+d} e^{-\sqrt{2}\chi}\right)^2$. That is why our models connect the T-model and the E-model in a different approximation.

E. General case

Finally, we discuss the following generic potential in Eq. (47). Similarly, the parameter V_0 can be determined by the constraint $A_s = 2.1 \times 10^{-9}$ at horizon crossing. There are three

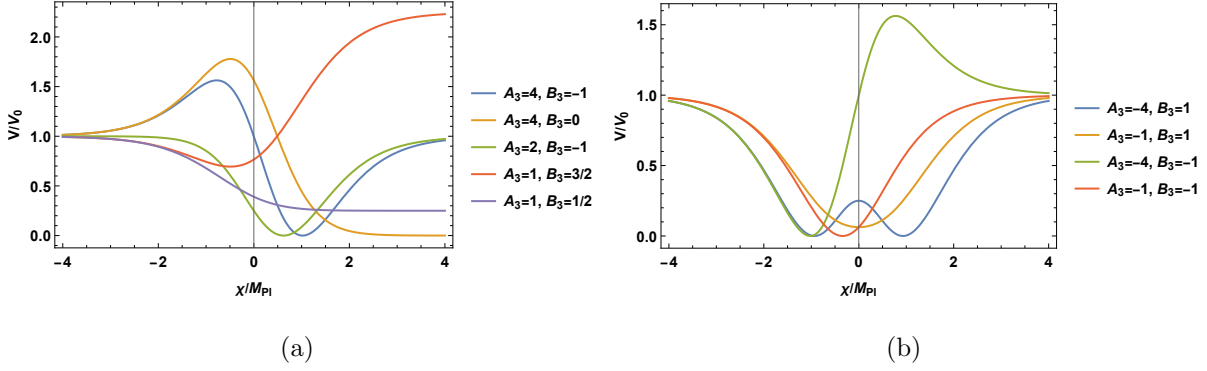


FIG. 25. Inflation potential in Eq. (47) with $A > 0$ (a) and $A < 0$ (b).

extreme points for the potential

$$\begin{aligned}
\chi_1 &= \frac{1}{\sqrt{2}} \log \left(\frac{A_3 - 2}{A_3 - 2B_3} \right), \\
\chi_2 &= \frac{1}{\sqrt{2}} \log \left(-\frac{\sqrt{A_3^2 - 4B_3} + A_3}{2B_3} \right), \\
\chi_3 &= \frac{1}{\sqrt{2}} \log \left(-\frac{A_3 - \text{sgn}(B_3)\sqrt{A_3^2 - 4B_3}}{2B_3} \right).
\end{aligned} \tag{67}$$

The potential with different parameters is shown in Fig. 25. For $A_3 > 2$ and $B_3 < 0$, the potential has a maximum at $\chi_M = \chi_1$ and a minimum at $\chi_m = \chi_3$. Similarly, inflation occurs in the regions $[\chi_M, \chi_m]$ and $[\chi_m, \infty]$ since the slow-roll conditions are violated in the region $[-\infty, \chi_M]$. The cosmological predictions in both regions are shown in Fig. 26. The slow-roll parameters and number of e -folding are

$$\begin{aligned}
\varepsilon &= \frac{4e^{2\sqrt{2}\chi} \left(\delta_0 - \delta_4 e^{\sqrt{2}\chi} \right)^2}{\left(e^{\sqrt{2}\chi} + 1 \right)^2 \left(1 + A_3 e^{\sqrt{2}\chi} + B_3 e^{2\sqrt{2}\chi} \right)^2}, \\
\eta &= \frac{4e^{\sqrt{2}\chi} \left(\delta_0 + 2\delta_1 e^{\sqrt{2}\chi} - 3\delta_2 e^{2\sqrt{2}\chi} + 2\delta_3 e^{3\sqrt{2}\chi} + B_3 \delta_4 e^{4\sqrt{2}\chi} \right)}{\left(e^{\sqrt{2}\chi} + 1 \right)^2 \left(1 + A_3 e^{\sqrt{2}\chi} + B_3 e^{2\sqrt{2}\chi} \right)^2}, \\
N &= \frac{1}{4} \left(-\frac{1}{\delta_0} e^{-\sqrt{2}\chi} - \frac{B_3}{\delta_4} e^{\sqrt{2}\chi} + \frac{\sqrt{2}\gamma_1}{\delta_0^2} \chi - \frac{2\gamma_2}{\delta_0^2 \delta_4^2} \log \left(e^{\sqrt{2}\chi} \delta_4 - \delta_0 \right) \right),
\end{aligned} \tag{68}$$

where $\delta_0 = A_3 - 2$, $\delta_1 = A_3^2 - 5A_3 + 2B_3 + 4$, $\delta_2 = 2A_3^2 - 3A_3(B_3 + 1) + 4B_3$, $\delta_3 = A_3^2 - 5A_3B_3 + 2B_3(2B_3 + 1)$, $\delta_4 = A_3 - 2B_3$, $\gamma_1 = A_3^2 - 2B_3 - 2$, and $\gamma_2 = (A_3^2 - 4B_3)(-A_3 + B_3 + 1)^2$. In order to obtain a prediction within the 2σ region of the Planck results, we need $B_3 \lesssim -450$.

Then these new parameters are approximated to be

$$\delta_1 \sim 2B_3, \quad \delta_2 \sim (4 - 3A_3)B_3, \quad \delta_3 \sim 4B_3^2, \quad \delta_4 \sim -2B_3.$$

Thus, the tensor-to-scalar ratio approximately is

$$r = 16\varepsilon \simeq \frac{4\delta_4^2}{(B_3 e^{\sqrt{2}\chi})^2} \sim 256e^{-2\sqrt{2}\chi}.$$

In the region $[\chi_M, \chi_m]$, the pivot scale leaves the horizon at $\chi_* \sim -5M_{\text{Pl}}$, and the tensor-to-scalar ratio is 10^{-4} , which is consistent with numerical calculations. Moreover, in the limit $B_3 \rightarrow -\infty$, the slow-roll parameters are independent on the parameter A_3 . Thus, the predictions are $n_s \simeq 0.9608, r \simeq 3.8 \times 10^{-4}$ for $N = 50$ and $n_s \simeq 0.9672, r \simeq 2.7 \times 10^{-4}$ for $N = 60$, which locate in the 2σ region of the Planck results and are shown as circles in Fig. 26(a). In the figure, the black scatters of the numerical predictions form a fan where the two boundaries and vertex of the fan come from the limits $A_3 \rightarrow 2, A_3 \rightarrow \infty$ and $B_3 \rightarrow -\infty$, respectively. There is a minimum at $\chi_m = \chi_3$ for the potential as setting $A_3 = 2$ and $B_3 < 0$, so there are two inflationary trajectories for which the predicted n_s and r are also shown in Fig. 26.

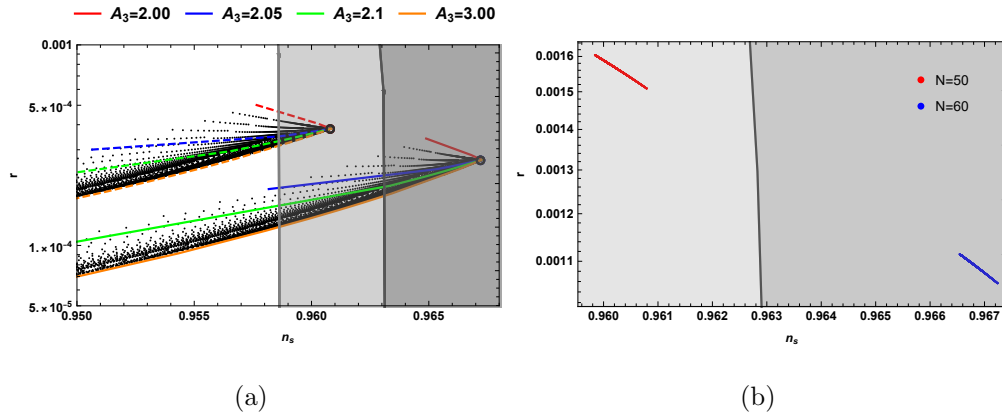


FIG. 26. The r versus n_s predictions for the inflaton potential in Eq. (47) with $A_3 \geq 2$ and $B_3 < 0$. (a) In the region $[\chi_M, \chi_m]$; the circles are in the limit $B_3 \rightarrow -\infty$. The dashed and solid lines are corresponding to $N = 50$ and $N = 60$. (b) In the region $[\chi_m, \infty]$.

When the parameters are in the region $A_3 > 2, B_3 > 0$, and $A_3 > 2B_3$, the potential has a maximum at $\chi_M = \chi_1$. Inflation can occur on both sides of the maximum where the predicted n_s and r are shown in Fig. 27. In order to get predictions which are consistent with the experimental data, the parameters should be $A_3 \simeq B_3$ or $A_3 \simeq 2, B_3 \sim 0$. While for $0 \leq A_3 < 2$, and $A_3 < 2B_3$, inflation can occur on the right side of the minimum $\chi_m = \chi_1$ for which the predicted n_s and r are shown in Fig. 28.

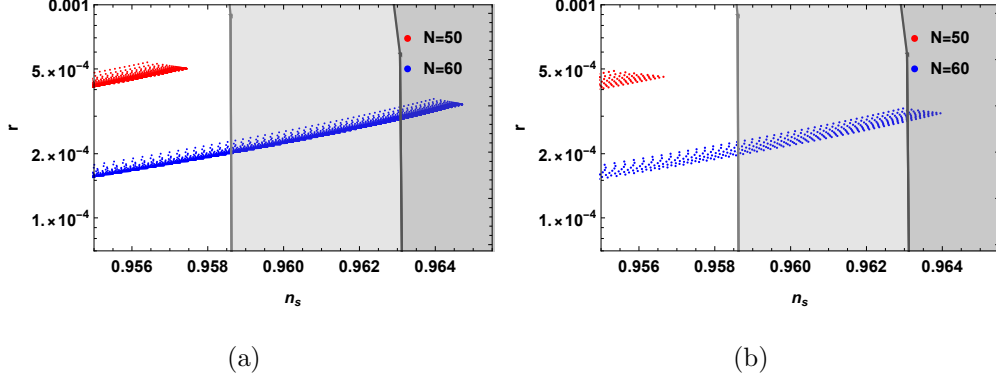


FIG. 27. The r versus n_s predictions for the inflaton potential in Eq. (47) with $A_3 > 2$, $B_3 > 0$, and $A_3 > 2B_3$. (a) In the region $[-\infty, \chi_M]$. (b) In the region $[\chi_M, \infty]$.

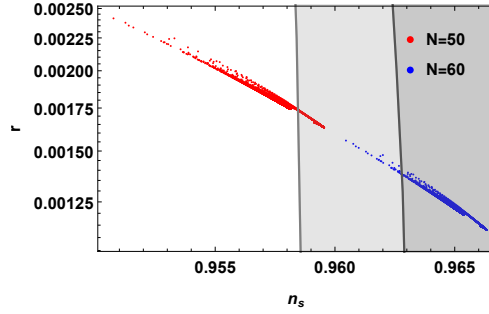


FIG. 28. CMB observations for the model in Eq. (47) with $0 \leq A_3 < 2$, $A_3 < 2B_3$. Inflation occurs on the right side of χ_m .

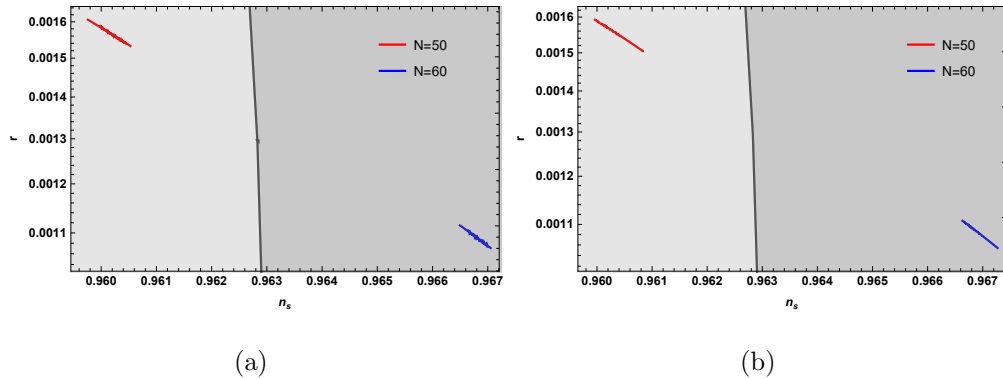


FIG. 29. The r versus n_s predictions for the inflaton potential in Eq. (47) with $A_3 < 0$, $B_3 > 0$, and $A_3^2 > 4B_3$. Inflation occurs in the regions (a) $[-\infty, \chi_{m1}]$ and (b) $[\chi_{m2}, \infty]$.

There are two minima at $\chi_{m1} = \chi_2$ and $\chi_{m2} = \chi_3$ and one maximum at $\chi_M = \chi_1$ for the potential with $A_3 < 0$, $B_3 > 0$, and $A_3^2 > 4B_3$. Inflation occurs in the regions $[-\infty, \chi_{m1}]$

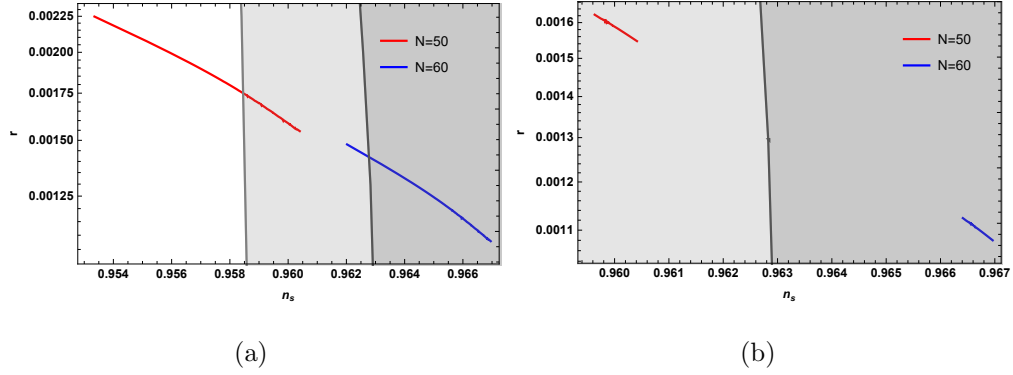


FIG. 30. The r versus n_s predictions for the inflaton potential in Eq. (47) with $A_3 < 0$, $B_3 > 0$, and $A_3^2 < 4B_3$. Inflation occurs in the regions (a) $[-\infty, \chi_m]$ and (b) $[\chi_m, \infty]$.

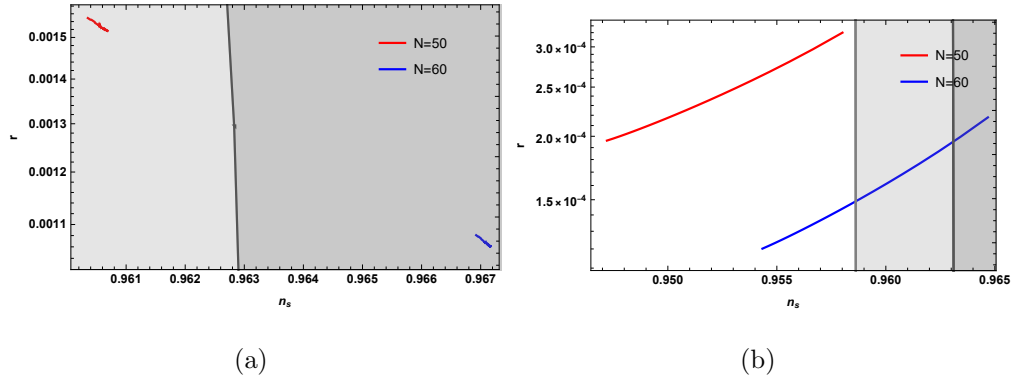


FIG. 31. The r versus n_s predictions for the inflaton potential in Eq. (47) with $A_3 < 0$, $B_3 < 0$, and $A_3 < 2B_3$. Inflation occurs in the regions (a) $[-\infty, \chi_m]$ and (b) $[\chi_m, \chi_M]$.

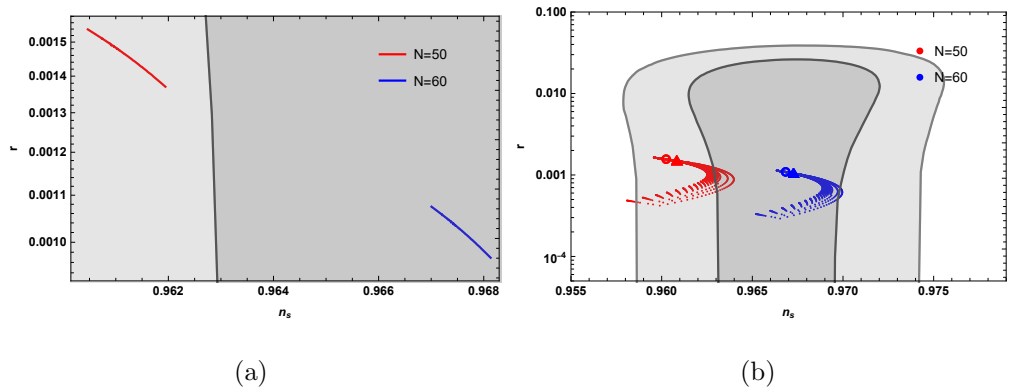


FIG. 32. The r versus n_s predictions for the inflaton potential in Eq. (47) with $A_3 < 0$, $B_3 < 0$, and $A_3 > 2B_3$. Inflation occurs in the regions (a) $[-\infty, \chi_m]$ and (b) $[\chi_m, \infty]$. The circles and triangles correspond to T- and E-models, respectively.

and $[\chi_{m2}, \infty]$, except the regions $[\chi_{m1}, \chi_M]$ and $[\chi_M, \chi_{m2}]$, where slow-roll inflation cannot

be realized due to $\eta > 1$ at χ_M . The predicted n_s and r are shown in Fig. 29. Moreover, inflation can happen on both the left and right sides of the minimum $\chi_m = \chi_1$ for the potential with $A_3 < 0$, $B_3 > 0$, $A_3^2 < 4B_3$, where the predicted n_s and r are shown in Fig. 30. while for $A_3 < 0$, $B_3 < 0$, and $A_3 < 2B_3$, the potential is a maximum at $\chi_M = \chi_1$ and a minimum at $\chi_m = \chi_3$. Similarly, the possible inflationary trajectories are in the regions $[-\infty, \chi_m]$ and $[\chi_m, \chi_M]$, and the predicted n_s and r are shown in Fig. 31. Especially, the relationship for parameters is $A \sim 2B$ in the region $[\chi_m, \chi_M]$. At last, for $A_3 < 0$, $B_3 < 0$, and $A_3 > 2B_3$, the potential only has one minimum at $\chi_m = \chi_3$, and the predicted n_s and r are shown in Fig. 32. On the right side of the minimum, the predictions of T- and E-models can also be covered. For the rest of the parameter spaces, there is no extreme point for the potential, and the slow-roll inflation is not possible on any trajectories.

VII. CONCLUSION

We have studied three classes of no-scale inflation models with one, two, and three moduli which can be realized naturally via string compactifications. Also, we considered the general renormalizable superpotential as a three-order polynomials of the inflaton field. The E-model and T-model for a fixed α are realized in the one modulus model and the three moduli model, respectively. They are connected by the three moduli model in the limits $2a_2\sqrt{c_1}/a_1 \rightarrow 1$ and $2a_2\sqrt{c_1}/a_1 \rightarrow \infty$. The detailed analyses of the spectral indices and the tensor-to-scalar ratio have been performed, and they are consistent with the Planck and BICEP/Keck experimental data on the cosmic microwave background. The spectral index is $n_s \simeq 1 - 2/N \sim 0.965$ for all models. Similar to the Starobinsky model, the tensor-to-scalar ratio r in the one and three moduli models are $r \simeq 2/(b^2 N^2)$, whereas r predicted in the two moduli models are $r \simeq 83/N^4$ due to the non-negligible contribution from the higher order term in potential. The parameter b is defined in terms of N_1 as $d = 1/\sqrt{2N_1}$. Thus, we have $b = 1/\sqrt{6}$ for one modulus models and $b = 1/\sqrt{2}$ for three moduli models. The tensor-to-scalar ratio in models with quartic and quadratic potential is significantly suppressed in no-scale supergravity, and then they can satisfy the strong bound from the current observations $r_{0.05} < 0.036$. In other words, no-scale supergravity is a viable framework which makes the excluded models valid again. In the three moduli model, the scalar potential is similar to that in global supersymmetry, but the Kähler potential is different. Thus, such no-scale

supergravity becomes a bridge between supergravity and global supersymmetry.

ACKNOWLEDGMENTS

This work is supported in part by the National Key Research and Development Program of China Grant No. 2020YFC2201504, by the Projects No. 11875062, No. 11947302, and No. 12047503 supported by the National Natural Science Foundation of China, by the Major Program of the National Natural Science Foundation of China under Grant No. 11690021, as well as by the Key Research Program of the Chinese Academy of Sciences, Grant No. XDPB15.

-
- [1] A. A. Starobinsky, A New Type of Isotropic Cosmological Models Without Singularity, *Phys. Lett. B* **91**, 99 (1980).
 - [2] A. H. Guth, The Inflationary Universe: A Possible Solution to the Horizon and Flatness Problems, *Phys. Rev. D* **23**, 347 (1981).
 - [3] A. D. Linde, A New Inflationary Universe Scenario: A Possible Solution of the Horizon, Flatness, Homogeneity, Isotropy and Primordial Monopole Problems, *Phys. Lett. B* **108**, 389 (1982).
 - [4] A. Albrecht and P. J. Steinhardt, Cosmology for Grand Unified Theories with Radiatively Induced Symmetry Breaking, *Phys. Rev. Lett.* **48**, 1220 (1982).
 - [5] D. H. Lyth and A. Riotto, Particle physics models of inflation and the cosmological density perturbation, *Phys. Rept.* **314**, 1 (1999), [arXiv:hep-ph/9807278](#).
 - [6] Y. Akrami *et al.* (Planck Collaboration), Planck 2018 results. X. Constraints on inflation, *Astron. Astrophys.* **641**, A10 (2020), [arXiv:1807.06211 \[astro-ph.CO\]](#).
 - [7] P. A. R. Ade *et al.* (BICEP and Keck Array Collaborations), Improved Constraints on Primordial Gravitational Waves using Planck, WMAP, and BICEP/Keck Observations through the 2018 Observing Season, *Phys. Rev. Lett.* **127**, 151301 (2021), [arXiv:2110.00483 \[astro-ph.CO\]](#).
 - [8] C. P. Burgess, M. Cicoli, and F. Quevedo, String Inflation After Planck 2013, *J. Cosmol. Astropart. Phys.* **11** (2013) 003, [arXiv:1306.3512 \[hep-th\]](#).

- [9] S. Bhattacharya, K. Dutta, M. R. Gangopadhyay, and A. Maharana, Confronting Kähler moduli inflation with CMB data, *Phys. Rev. D* **97**, 123533 (2018), [arXiv:1711.04807 \[astro-ph.CO\]](#).
- [10] M. Cicoli, V. A. Diaz, and F. G. Pedro, Primordial Black Holes from String Inflation, *J. Cosmol. Astropart. Phys.* **06** (2018) 034, [arXiv:1803.02837 \[hep-th\]](#).
- [11] R. Kallosh and A. Linde, BICEP/Keck and cosmological attractors, *J. Cosmol. Astropart. Phys.* **12** (2021) 008, [arXiv:2110.10902 \[astro-ph.CO\]](#).
- [12] J. Ellis, M. A. G. Garcia, D. V. Nanopoulos, K. A. Olive, and S. Verner, BICEP/Keck constraints on attractor models of inflation and reheating, *Phys. Rev. D* **105**, 043504 (2022), [arXiv:2112.04466 \[hep-ph\]](#).
- [13] E. J. Copeland, A. R. Liddle, D. H. Lyth, E. D. Stewart, and D. Wands, False vacuum inflation with Einstein gravity, *Phys. Rev. D* **49**, 6410 (1994), [arXiv:astro-ph/9401011](#).
- [14] E. D. Stewart, Inflation, supergravity and superstrings, *Phys. Rev. D* **51**, 6847 (1995), [arXiv:hep-ph/9405389](#).
- [15] M. Dine, L. Randall, and S. D. Thomas, Supersymmetry breaking in the early universe, *Phys. Rev. Lett.* **75**, 398 (1995), [arXiv:hep-ph/9503303](#).
- [16] E. Cremmer, S. Ferrara, C. Kounnas, and D. V. Nanopoulos, Naturally Vanishing Cosmological Constant in N=1 Supergravity, *Phys. Lett. B* **133**, 61 (1983).
- [17] J. R. Ellis, A. B. Lahanas, D. V. Nanopoulos, and K. Tamvakis, No-Scale Supersymmetric Standard Model, *Phys. Lett. B* **134**, 429 (1984).
- [18] A. B. Lahanas and D. V. Nanopoulos, The Road to No Scale Supergravity, *Phys. Rept.* **145**, 1 (1987).
- [19] E. Witten, Dimensional Reduction of Superstring Models, *Phys. Lett. B* **155**, 151 (1985).
- [20] T.-j. Li, J. L. Lopez, and D. V. Nanopoulos, Compactifications of M-theory and their phenomenological consequences, *Phys. Rev. D* **56**, 2602 (1997), [arXiv:hep-ph/9704247](#).
- [21] J. Ellis, D. V. Nanopoulos, and K. A. Olive, No-Scale Supergravity Realization of the Starobinsky Model of Inflation, *Phys. Rev. Lett.* **111**, 111301 (2013), [Erratum: *Phys.Rev.Lett.* **111**, 129902 (2013)], [arXiv:1305.1247 \[hep-th\]](#).
- [22] J. Ellis, D. V. Nanopoulos, and K. A. Olive, Starobinsky-like Inflationary Models as Avatars of No-Scale Supergravity, *J. Cosmol. Astropart. Phys.* **10** (2013) 009, [arXiv:1307.3537 \[hep-th\]](#).

- [23] J. Ellis, M. A. G. Garcia, D. V. Nanopoulos, and K. A. Olive, No-Scale Inflation, *Class. Quant. Grav.* **33**, 094001 (2016), [arXiv:1507.02308 \[hep-ph\]](#).
- [24] J. Ellis, M. A. G. Garcia, N. Nagata, D. V. Nanopoulos, K. A. Olive, and S. Verner, Building models of inflation in no-scale supergravity, *Int. J. Mod. Phys. D* **29**, 2030011 (2020), [arXiv:2009.01709 \[hep-ph\]](#).
- [25] M. Kawasaki, M. Yamaguchi, and T. Yanagida, Natural chaotic inflation in supergravity, *Phys. Rev. Lett.* **85**, 3572 (2000), [arXiv:hep-ph/0004243](#).
- [26] M. Yamaguchi and J. Yokoyama, New inflation in supergravity with a chaotic initial condition, *Phys. Rev. D* **63**, 043506 (2001), [arXiv:hep-ph/0007021](#).
- [27] M. Yamaguchi, Natural double inflation in supergravity, *Phys. Rev. D* **64**, 063502 (2001), [arXiv:hep-ph/0103045](#).
- [28] M. Kawasaki and M. Yamaguchi, A Supersymmetric topological inflation model, *Phys. Rev. D* **65**, 103518 (2002), [arXiv:hep-ph/0112093](#).
- [29] R. Kallosh and A. Linde, New models of chaotic inflation in supergravity, *J. Cosmol. Astropart. Phys.* **11** (2010) 011, [arXiv:1008.3375 \[hep-th\]](#).
- [30] R. Kallosh, A. Linde, and T. Rube, General inflaton potentials in supergravity, *Phys. Rev. D* **83**, 043507 (2011), [arXiv:1011.5945 \[hep-th\]](#).
- [31] T. Li, Z. Li, and D. V. Nanopoulos, Supergravity Inflation with Broken Shift Symmetry and Large Tensor-to-Scalar Ratio, *J. Cosmol. Astropart. Phys.* **02** (2014) 028, [arXiv:1311.6770 \[hep-ph\]](#).
- [32] K. Nakayama, F. Takahashi, and T. T. Yanagida, Polynomial Chaotic Inflation in the Planck Era, *Phys. Lett. B* **725**, 111 (2013), [arXiv:1303.7315 \[hep-ph\]](#).
- [33] K. Nakayama, F. Takahashi, and T. T. Yanagida, Polynomial Chaotic Inflation in Supergravity, *J. Cosmol. Astropart. Phys.* **08** (2013) 038, [arXiv:1305.5099 \[hep-ph\]](#).
- [34] F. Takahashi, New inflation in supergravity after Planck and LHC, *Phys. Lett. B* **727**, 21 (2013), [arXiv:1308.4212 \[hep-ph\]](#).
- [35] T. Li, Z. Li, and D. V. Nanopoulos, Natural Inflation with Natural Trans-Planckian Axion Decay Constant from Anomalous $U(1)_X$, *J. High Energy Phys.* **07** (2014) 052, [arXiv:1405.1804 \[hep-th\]](#).
- [36] C. Pallis and Q. Shafi, From Hybrid to Quadratic Inflation With High-Scale Supersymmetry Breaking, *Phys. Lett. B* **736**, 261 (2014), [arXiv:1405.7645 \[hep-ph\]](#).

- [37] T. Li, Z. Li, and D. V. Nanopoulos, Symmetry Breaking Indication for Supergravity Inflation in Light of the Planck 2015, *J. Cosmol. Astropart. Phys.* **09** (2015) 006, [arXiv:1502.05005 \[hep-ph\]](#).
- [38] T. Li, Z. Li, and D. V. Nanopoulos, Helical Phase Inflation, *Phys. Rev. D* **91**, 061303 (2015), [arXiv:1409.3267 \[hep-th\]](#).
- [39] T. Li, Z. Li, and D. V. Nanopoulos, Helical Phase Inflation and Monodromy in Supergravity Theory, *Adv. High Energy Phys.* **2015**, 397410 (2015), [arXiv:1412.5093 \[hep-th\]](#).
- [40] T. Li, Z. Li, and D. V. Nanopoulos, Helical Phase Inflation via Non-Geometric Flux Compactifications: from Natural to Starobinsky-like Inflation, *J. High Energy Phys.* **10** (2015) 138, [arXiv:1507.04687 \[hep-th\]](#).
- [41] M. Sabir, W. Ahmed, Y. Gong, T. Li, and J. Lin, Helical phase inflation and its observational constraints, *J. Cosmol. Astropart. Phys.* **09** (2020) 038, [arXiv:1908.05201 \[hep-ph\]](#).
- [42] B. J. Broy, D. Ciupke, F. G. Pedro, and A. Westphal, Starobinsky-Type Inflation from α' -Corrections, *J. Cosmol. Astropart. Phys.* **01** (2016) 001, [arXiv:1509.00024 \[hep-th\]](#).
- [43] J. Ellis, N. E. Mavromatos, and D. V. Nanopoulos, Starobinsky-Like Inflation in Dilaton-Brane Cosmology, *Phys. Lett. B* **732**, 380 (2014), [arXiv:1402.5075 \[hep-th\]](#).
- [44] M. Cicoli, F. G. Pedro, and G. Tasinato, Poly-instanton Inflation, *J. Cosmol. Astropart. Phys.* **12** (2011) 022, [arXiv:1110.6182 \[hep-th\]](#).
- [45] X. Gao and P. Shukla, On Non-Gaussianities in Two-Field Poly-Instanton Inflation, *J. High Energy Phys.* **03** (2013) 061, [arXiv:1301.6076 \[hep-th\]](#).
- [46] M. Cicoli, S. Downes, and B. Dutta, Power Suppression at Large Scales in String Inflation, *J. Cosmol. Astropart. Phys.* **12** (2013) 007, [arXiv:1309.3412 \[hep-th\]](#).
- [47] T. Kobayashi, S. Uemura, and J. Yamamoto, Polyinstanton axion inflation, *Phys. Rev. D* **96**, 026007 (2017), [arXiv:1705.04088 \[hep-ph\]](#).
- [48] S. Bhattacharya, K. Dutta, M. R. Gangopadhyay, A. Maharana, and K. Singh, Fibre Inflation and Precision CMB Data, *Phys. Rev. D* **102**, 123531 (2020), [arXiv:2003.05969 \[astro-ph.CO\]](#).
- [49] M. Cicoli and E. Di Valentino, Fitting string inflation to real cosmological data: The fiber inflation case, *Phys. Rev. D* **102**, 043521 (2020), [arXiv:2004.01210 \[astro-ph.CO\]](#).
- [50] M. Cicoli, F. G. Pedro, and N. Pedron, Secondary GWs and PBHs in string inflation: formation and detectability, [arXiv:2203.00021 \[hep-th\]](#).

- [51] R. Kallosh, A. Linde, and D. Roest, Superconformal Inflationary α -Attractors, *J. High Energ. Phys.* **11** (2013) 198, [arXiv:1311.0472 \[hep-th\]](#).
- [52] R. Kallosh and A. Linde, Planck, LHC, and α -attractors, *Phys. Rev. D* **91**, 083528 (2015), [arXiv:1502.07733 \[astro-ph.CO\]](#).
- [53] A. Linde, Single-field α -attractors, *J. Cosmol. Astropart. Phys.* **05** (2015) 003, [arXiv:1504.00663 \[hep-th\]](#).
- [54] A. Linde, Random Potentials and Cosmological Attractors, *J. Cosmol. Astropart. Phys.* **02** (2017) 028, [arXiv:1612.04505 \[hep-th\]](#).
- [55] J. Ellis, D. V. Nanopoulos, K. A. Olive, and S. Verner, Unified No-Scale Attractors, *J. Cosmol. Astropart. Phys.* **09** (2019) 040, [arXiv:1906.10176 \[hep-th\]](#).
- [56] Y. Tang and Y.-L. Wu, Conformal α -attractor inflation with Weyl gauge field, *J. Cosmol. Astropart. Phys.* **03** (2020) 067, [arXiv:1912.07610 \[hep-ph\]](#).
- [57] Y. Akrami, S. Casas, S. Deng, and V. Vardanyan, Quintessential α -attractor inflation: forecasts for Stage IV galaxy surveys, *J. Cosmol. Astropart. Phys.* **04** (2021) 006, [arXiv:2010.15822 \[astro-ph.CO\]](#).
- [58] J. G. Rodrigues, S. Santos da Costa, and J. S. Alcaniz, Observational constraints on α - attractor inflationary models with a Higgs-like potential, *Phys. Lett. B* **815**, 136156 (2021), [arXiv:2007.10763 \[astro-ph.CO\]](#).
- [59] T.-j. Li, Compactification and supersymmetry breaking in M theory, *Phys. Rev. D* **57**, 7539 (1998), [arXiv:hep-th/9801123](#).
- [60] T. Li, Z. Li, and D. V. Nanopoulos, Chaotic Inflation in No-Scale Supergravity with String Inspired Moduli Stabilization, *Eur. Phys. J. C* **75**, 55 (2015), [arXiv:1405.0197 \[hep-th\]](#).
- [61] L. Wu, Y. Gong, and T. Li, Primordial black holes and secondary gravitational waves from string inspired general no-scale supergravity, *Phys. Rev. D* **104**, 123544 (2021), [arXiv:2105.07694 \[gr-qc\]](#).
- [62] M. K. Gaillard, H. Murayama, and K. A. Olive, Preserving flat directions during inflation, *Phys. Lett. B* **355**, 71 (1995), [arXiv:hep-ph/9504307](#).
- [63] G. A. Diamandis, J. R. Ellis, A. B. Lahanas, and D. V. Nanopoulos, Vanishing Scalar Masses in No Scale Supergravity, *Phys. Lett. B* **173**, 303 (1986).
- [64] I. Garg and S. Mohanty, No scale SUGRA SO(10) derived Starobinsky Model of Inflation, *Phys. Lett. B* **751**, 7 (2015), [arXiv:1504.07725 \[hep-ph\]](#).

- [65] I. Garg and S. Mohanty, No-scale SUGRA Inflation and Type-I seesaw, *Int. J. Mod. Phys. A* **33**, 1850127 (2018), [arXiv:1711.01979 \[hep-ph\]](#).
- [66] S. Khalil, A. Moursy, A. K. Saha, and A. Sil, $U(1)_R$ inspired inflation model in no-scale supergravity, *Phys. Rev. D* **99**, 095022 (2019), [arXiv:1810.06408 \[hep-ph\]](#).
- [67] A. D. Linde, Chaotic Inflation, *Phys. Lett. B* **129**, 177 (1983).
- [68] P. Creminelli, S. Dubovsky, D. López Nacir, M. Simonović, G. Trevisan, G. Villadoro, and M. Zaldarriaga, Implications of the scalar tilt for the tensor-to-scalar ratio, *Phys. Rev. D* **92**, 123528 (2015), [arXiv:1412.0678 \[astro-ph.CO\]](#).
- [69] T. Li, Z. Sun, C. Tian, and L. Wu, The Renormalizable Three-Term Polynomial Inflation with Large Tensor-to-Scalar Ratio, *Eur. Phys. J. C* **75**, 301 (2015), [arXiv:1407.8063 \[hep-ph\]](#).